

Towards Large-Scale Small Object Detection: Survey and Benchmarks

Gong Cheng, Xiang Yuan, Xiwen Yao, Kebing Yan, Qinghua Zeng, and Junwei Han, *Fellow, IEEE*

Abstract—With the rise of deep convolutional neural networks, object detection has achieved prominent advances in past years. However, such prosperity could not camouflage the unsatisfactory situation of Small Object Detection (SOD), one of the notoriously challenging tasks in computer vision, owing to the poor visual appearance and noisy representation caused by the intrinsic structure of small targets. In addition, large-scale dataset for benchmarking small object detection methods remains a bottleneck. In this paper, we first conduct a thorough review of small object detection. Then, to catalyze the development of SOD, we construct two large-scale Small Object Detection dAtsets (SODA), SODA-D and SODA-A, which focus on the Driving and Aerial scenarios respectively. SODA-D includes 24704 high-quality traffic images and 277596 instances of 9 categories. For SODA-A, we harvest 2510 high-resolution aerial images and annotate 800203 instances over 9 classes. The proposed datasets, as we know, are the first-ever attempt to large-scale benchmarks with a vast collection of exhaustively annotated instances tailored for multi-category SOD. Finally, we evaluate the performance of mainstream methods on SODA. We expect the released benchmarks could facilitate the development of SOD and spawn more breakthroughs in this field. Datasets and codes will be available soon at: <https://shaunyuan22.github.io/SODA>.

Index Terms—Object detection, Small object detection, Deep learning, Convolutional neural networks, Benchmark.

1 INTRODUCTION

OBJECT detection is an essential task which aims at categorizing and locating the objects of interest in images/videos. Thanks to the enormous volume of data and powerful learning ability of deep Convolutional Neural Networks (CNNs), object detection has scored remarkable achievements in recent years [1], [2], [3], [4], [5]. Small ¹ Object Detection (SOD), as a sub-field of generic object detection, which concentrates on detecting those objects with small size, is of great theoretical and practical significance in various scenarios such as surveillance, drone scene analysis, pedestrian detection, traffic sign detection in autonomous driving, *etc.*

Albeit the substantial progresses have been made in generic object detection, the research of SOD proceeded at a relatively slow pace. To be more specific, there remains a huge performance gap in detecting small and normal sized objects even for leading detectors. Taking DyHead [9], one of the state-of-the-art detectors, as an example, the mean Average Precision (mAP) metric of small objects on COCO [6] test-dev set obtained by DyHead is only 28.3%, significantly lag behind that of objects with medium and large sizes (50.3% and 57.5% respectively). We posit such performance degradation originates the following two-fold: 1) the intrinsic difficulty of learning proper representation from limited and distorted information of small objects; 2) the scarcity of large-scale dataset for small object detection.

The low-quality feature representation of small objects can be attributed to their limited sizes and the generic fea-

ture extraction paradigm. Concretely, the current prevailing feature extractors [10], [11], [12] usually down-sample the feature maps to diminish the spatial redundancy and learn high dimensional features, which unavoidably extinguishes the representation of tiny objects. Moreover, the features of small objects are inclined to be contaminated by background and other instances after the convolution process, making the network can hardly capture the discriminative information that is pivotal for the subsequent tasks. To tackle this problem, researchers have proposed a series of work, which can be categorized into 6 groups: data-manipulation methods, scale-aware methods, feature-fusion methods, super-resolution methods, context-modeling methods, and other approaches. We will discuss these approaches exhaustively in the review part and in-depth analyses will be provided too.

To alleviate the data scarcity, some datasets tailored for small object detection have been proposed, *e.g.*, SOD [28] and TinyPerson [7]. However, these small-scale datasets cannot meet the needs of training supervised CNN-based algorithms, which are “hungry” for a substantial amount of labeled data. In addition, several public datasets contain a considerable number of small objects, such as WiderFace [8], SeaPerson [29] and DOTA [30], *etc.* Unfortunately, these datasets are either designed for single-category detection task (face detection or pedestrian detection) which usually follows a relatively certain pattern, or among which tiny objects merely distribute in a few categories (*small-vehicle* in DOTA dataset). In a nutshell, the currently available datasets could not support the training of deep learning-based models customized for small object detection, as well as serve as an impartial benchmark for evaluating multi-category SOD algorithms. Whilst, as a foundation for building data-driven deep CNN models, the accessibility of large-scale datasets such as PASCAL VOC [31], ImageNet

• G. Cheng, X. Yuan, X. Yao, K. Yan, Q. Zeng and J. Han are with School of Automation, Northwestern Polytechnical University, Xi'an, 710021, China. Email: gcheng, yaoxiwen@nwpu.edu.cn, shaunyuan, kebingyan, zengqinghua@mail.nwpu.edu.cn, junweihan2010@gmail.com
• Junwei Han is the corresponding author.

1. Here by “small” we mean the size of the object is relatively limited and often determined by an area [6] or length [7], [8] threshold.

TABLE 1

Summary of several surveys related to object detection. The top are the surveys focusing on the generic object detection and specific tasks, and the bottom are the existing reviews of small object detection.

Title	Publication	Descriptions
Deep Learning for Generic Object Detection: A Survey [13]	IJCV 2020	A comprehensive survey of the recent progresses driven by deep learning techniques in generic object detection
Object Detection With Deep Learning: A Review [14]	TNNLS 2019	A systematic review on deep learning-based detection frameworks for generic object detection and other subtasks
Survey of Pedestrian Detection for Advanced Driver Assistance Systems [15]	TPAMI 2009	A survey focuses on pedestrian detection in advanced driver assistance systems
Pedestrian detection: an evaluation of the state of the art [16]	TPAMI 2011	A detailed evaluation of pedestrian detectors in monocular images
From Handcrafted to Deep Features for Pedestrian Detection: A Survey [17]	TPAMI 2021	A thorough survey for pedestrian detection including handcrafted features based methods and deep features based approaches
Text Detection and Recognition in Imagery: A Survey [18]	TPAMI 2014	A systematic survey related to automatic text detection and recognition in color images
A survey on object detection in optical remote sensing images [19]	JPRS 2016	A review of recent progress about object detection in optical remote sensing images
Object detection in optical remote sensing images: A survey and a new benchmark [20]	JPRS 2020	A thorough review of deep learning based methods for object detection in aerial images
Vision for Looking at Traffic Lights: Issues, Survey, and Perspectives [21]	TITS 2016	An overview of traffic light recognition research in relation to driver assistance systems
Object Detection Using Deep Learning Methods in Traffic Scenarios [22]	ACM CS 2021	A survey dedicated to object detection in traffic scenarios based on deep learning methods
Imbalance Problems in Object Detection: A Review [23]	TPAMI 2020	A comprehensive review of the imbalance problems in object detection
Weakly Supervised Object Localization and Detection: A Survey [24]	TPAMI 2021	A systematic survey on weakly supervised object localization and detection
Recent advances in small object detection based on deep learning: A review [25]	IVC 2020	A review of existing detection methods which can be utilized for small objects in natural images based on deep learning
A survey and performance evaluation of deep learning methods for small object detection [26]	ESWA 2021	A survey of recently developed deep learning methods for small object detection
A Survey of the Four Pillars for Small Object Detection: Multiscale Representation, Contextual Information, Super-Resolution, and Region Proposal [27]	TSMCS 2022	A review of small object detection based on four genres of techniques: multiscale representation, contextual information, super-resolution, and region-proposal

[32], COCO [6], and DOTA [30] is of great significance for both the academic and industrial communities, and each of which noticeably boosts the development of object detection in related fields. This inspires us to think: can we build a large-scale dataset, where the objects of multiple categories have very limited sizes, to serve as a benchmark that can be adopted to verify the design of small object detection framework and facilitate the further research of SOD?

Taking the aforementioned problems into account, we construct two large-scale Small Object Detection dAtasets (SODA), SODA-D and SODA-A, which focus on the Driving and Aerial scenarios respectively. The proposed SODA-D is built on top of MVD [33] and our data, where the former is a dataset dedicated to pixel-level understanding of street scenes, and the latter is mainly captured by on-board cameras and mobile phones. With 24704 well-chosen and high-quality images of driving scenarios, we annotate 277596 instances of 9 categories with horizontal bounding boxes. SODA-A is the benchmark specialized for small object detection task under aerial scenes, which has 800203 instances with oriented rectangle box annotation across 9 classes. It contains 2510 high-resolution images extracted from Google Earth.

1.1 Comparisons with previous reviews

Quite a number of surveys about object detection have been published in recent years [13], [14], [15], [16], [17], [18], [19], [20], [21], [22], [23], [24], our review differs from the existing ones mainly in two aspects.

1. **A comprehensive and timely review dedicated to small object detection task across multiple domains.** Most of the previous reviews (as in Tab. 1) concentrate on either generic object detection [13], [14] or specific object detection task such as pedestrian detection [15], [16], [17], text detection [18], detection in remote sensing images [19], [20], and detection under traffic scenarios [21], [22], etc. Furthermore, there already exist several reviews paid their attention to small object detection [25], [26], [27], however, they fail to the comprehensiveness and in-depth analysis because only partial reviews on limited areas were conducted. By extensively reviewing hundreds of literature related to small

object detection which covers a broad spectrum of research fields, including face detection, pedestrian detection, traffic sign detection, vehicle detection, object detection in aerial images, to name a few, we provide a systematic survey of small object detection and an understandable taxonomy that organizes SOD approaches into six major categories based on the techniques used.

2. **Two large-scale benchmarks customized for small object detection were proposed, on which in-depth evaluation and analysis of several representative detection algorithms were performed.** We present the large-scale benchmark SODA that enables a thorough evaluation of several representative methods and moreover, we provide an impartial performance comparison and detailed analyses, which were lacking in the previous reviews.

1.2 Scope

Object detection in early period usually integrated hand-crafted features [34], [35], [36] and machine learning approaches [37], [38] to recognize the objects of interest. The methods following this sophisticated philosophy perform catastrophically poorly in small objects due to their limited capability of scale variation. After 2012, the powerful learning ability of deep convolutional network [39] brings a glimmer of hope to the whole detection community, especially considering that object detection had reached a plateau after 2010 [40]. The seminal work [40] broken the ice and since then, an increasing number of detection methods based on deep neural networks were proposed, whereafter, object detection entering the deep learning era. Thanks to the outstanding modeling ability of deep networks for scale variation and powerful abstraction of information, small object detection obtains an unprecedented improvement. Therefore, our review focuses on the major development of deep learning-based SOD methods.

To sum up, the main contributions of this paper are in three folds:

1. Reviewing the development of small object detection in the deep-learning era and providing a systematic survey of the recent progress in this field, which can be grouped into 6 categories: data-manipulation methods, scale-aware

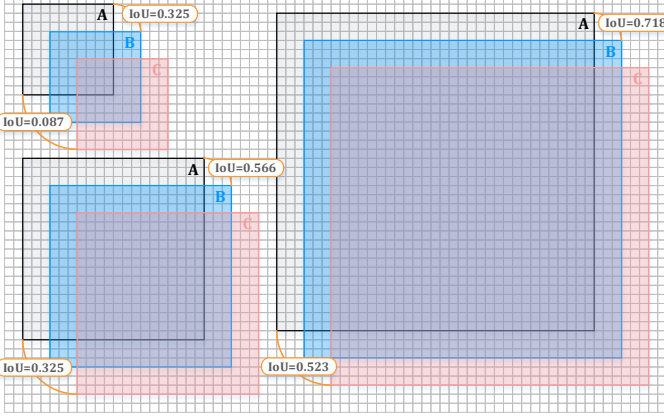


Fig. 1. Low tolerance of small objects for bounding box perturbation. Top-left, bottom-left and right represent small object (20×20 pixels), a grid denotes two pixels), medium object (40×40 pixels) and large object (70×70 pixels), respectively. **A** denotes the Ground Truth (GT) box, **B** and **C** stand for predicted boxes with slight deviations along the diagonal direction (6 pixels and 12 pixels, respectively). IoU indicates the Intersection-over-Union value between the GT box and the related predicted box.

methods, feature-fusion methods, super-resolution methods, context-modeling methods, and other approaches. Except for the taxonomies, in-depth analysis about the pros and cons of these methods were also provided. Meanwhile, we review a dozen datasets that span over multiple areas which relate to small object detection.

2. Releasing two large-scale benchmarks for small object detection, where the first one was dedicated to driving scenarios and the other was specialized for aerial scenes. The proposed datasets are the first-ever attempt to large-scale benchmarks tailored for SOD. We hope these two exhaustively annotated benchmarks could help the researchers to develop and verify effective frameworks for SOD and facilitate more breakthroughs in this field.

3. Investigating the performance of several representative object detection methods on our datasets, and providing in-depth analyses according to the quantitative and qualitative results, which could benefit the algorithm design of small object detection afterwards.

The remainder of this paper is organized as follows. In Section 2, we conduct a comprehensive survey of small object detection. And a thorough review on several publicly available benchmarks related to small object detection is given in Section 3. In Section 4, we elaborate the collection and annotation process, as well as the data characteristics, about the proposed benchmarks. In Section 5, the results and analyses of several representative methods on our benchmarks are provided. Finally, we conclude our work and discuss the prospective research directions of small object detection.

2 REVIEW ON SMALL OBJECT DETECTION

2.1 Problem Definition

Object detection aims to classify and locate instances. Small object detection or tiny object detection, as the term suggests, merely focus on detecting those objects with limited sizes. In this task, the terms *tiny* and *small* are typically

defined by an area threshold [6] or length threshold [7], [8]. Take COCO [6] as an example, the objects occupying an area less than and equal to 1024 pixels come to *small* category. Considering that there is no unified and distinct definition about small objects so far, unless specified, in this Section, we follow the expressions about those *tiny* and *small* terms in the original papers, and it is worth noting that they are inconsistent with the definitions about *Tiny* and *Small* in our benchmarks, which will be introduced in Sec. 4.

2.2 Main Challenges

In addition to some common challenges in generic object detection such as intra-class variations, inaccurate localization, occluded object detection, *etc.*, typical issues exist when it comes to SOD tasks, primarily including object information loss, noisy feature representation and low tolerance for bounding box perturbation.

Information loss. Current prevailing object detectors [1], [2], [3], [4], [5], [9] usually include a backbone network and a detection head, where the latter makes decision depends on the representation output by the former. Such paradigm was proven to be effective and gives rise to the unprecedented success. However, the generic feature extractor [10], [11], [12] usually leverage sub-sampling operations to filter noisy activation [41] and reduce the spatial resolution of feature maps, thus inevitably losing the information of objects. Such information loss will scarcely impair the performance of large or medium-sized objects to a certain extent, considering that the final features still retain enough information of them. Unfortunately, this is fatal for small objects, because the detection head can hardly give accurate predictions on top of the highly structural representations, in which the weak signals of small objects were almost wiped out.

Noisy feature representation. Discriminative features are crucial for both the classification and localization tasks [42], [43]. Small objects often have low-resolution and poor-quality appearance, consequently it is intractable to learn representations with discrimination from their distorted structures. At the same time, the regional features of small objects are inclined to be contaminated by the background and other instances, introducing noise to the learned representation further. To sum up, the feature representations of small objects are apt to suffer from the noise, hindering the subsequent detection.

Low tolerance for bounding box perturbation. Localization, as one of the primary tasks of detection, is formulated as a regression problem in most detection paradigms, in which localization branch was designed to output the bounding box offsets [1], [3], [44], [45], [46] or the object size [4], [47], and generally the Intersection over Union (IoU) metric was adopted to evaluate the accuracy. Nevertheless, localizing small objects is tougher than larger ones. As shown in Fig. 1, a slight deviation (6 pixels along the diagonal direction) of predicted box for a small object causes significant drop on IoU (from 100% to 32.5%) compared to medium and large objects (56.6% and 71.8%). Meanwhile, a greater variance (say, 12 pixels) further exacerbates the situation, and the IoU drops to poorly 8.7% for small objects. That is to say, small objects have a lower tolerance for bounding box perturbation compared with larger ones, aggravating the learning of regression branch.

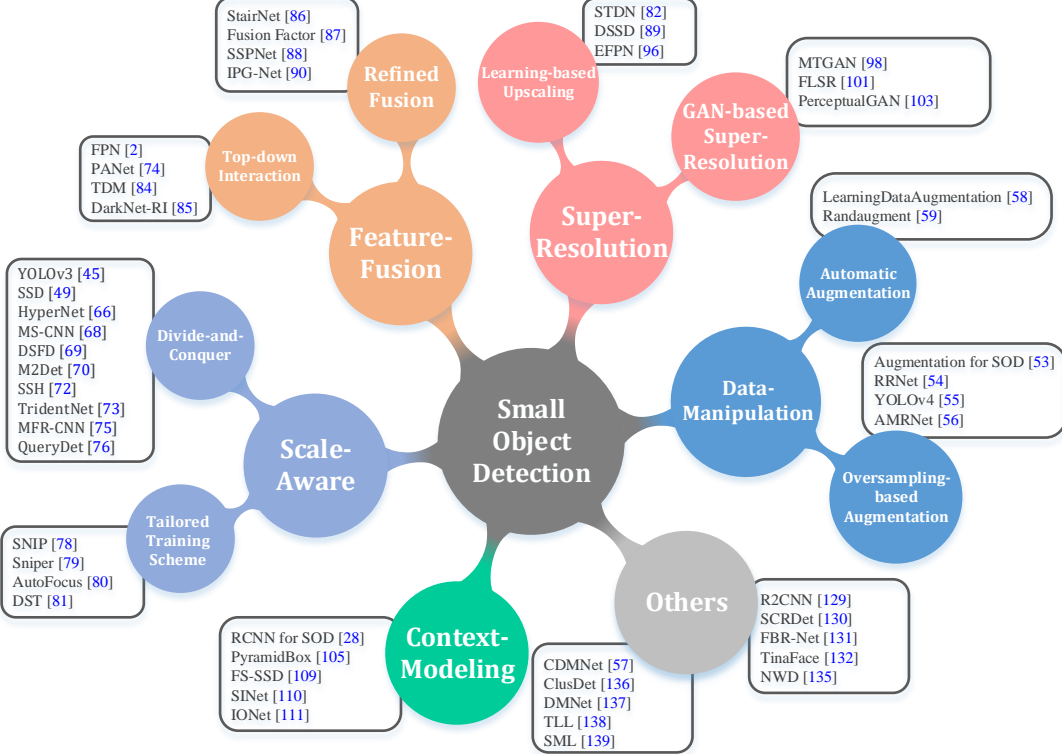


Fig. 2. Structured taxonomy of the existing deep learning-based methods for small object detection, which includes five major genres and other approaches. Only several representative methods of each category are demonstrated.

2.3 Review of Small Object Detection Algorithms

General object detection methods based on deep learning can be categorized into two groups: two-stage and one-stage detection, where the former detects objects in a coarse-to-fine routine while the latter performs the detection at one stroke. Two-stage detection methods [1], [46], [48] produce high-quality proposals with a well-designed architecture such as Region Proposal Network (RPN) [1] at first, then the detection heads take regional features as input and perform subsequent classification and localization respectively. Compared with two-stage algorithms, one-stage approaches [3], [44], [49] tile dense anchors on feature maps and predict the classification scores and coordinates directly. Benefiting from proposal-free setting, one-stage detectors enjoy high computational efficiency but often lag behind in accuracy. In addition to the above two categories, several anchor-free [4], [47], [50], [51] methods have emerged in recent years, which discard the anchor paradigm. Moreover, query-based detectors [5], [52], which formulate the detection as a set prediction task, have shown great potential. We cannot elaborate on the related frameworks in the light of space restraints. Please refer to corresponding surveys [13], [14] and original papers for more details.

To address the aforementioned challenging issues, existing small object detection methods usually introduce deliberate designs to current powerful paradigms which work well in generic object detection. Next, we will briefly introduce these approaches and an overview of the proposed solutions is presented in Fig. 2.

2.3.1 Data-manipulation methods

General object detection methods have to strike a balance between objects of different scales, where the targets with

tiny sizes only occupy a small portion in current datasets [6], [30], [31]. Such scale-level imbalance hampers the performance of detectors on small objects to a certain extent and an intuitive solution is to increase the number of small objects. Follow this line, a series of work have been proposed and can be broadly categorized into two categories: oversampling-based augmentation strategy and automatic augmentation scheme.

Oversampling-based augmentation strategy. Kisantal *et al.* [53] adopted an augmentation strategy by copying a small object and pasting it with random transformation to different positions in the identical image. RRNet [54] introduces an adaptive augmentation strategy named AdaResampling, which follows the same philosophy as [53], the major difference lies in that a prior segmentation map was used to guide the sample process of valid positions to be pasted, and a scale transformation for pasted objects reduces the scale discrepancy further. In [55], [56], [57], a new data augmentation strategy Mosaic was proposed to augment the original data, which stitches several (*e.g.*, 4) images to form a new sample. This operation improves the number of small instances in practice owing to the original images were generally shrunk to a smaller size.

Automatic augmentation scheme. The methods following this paradigm explore an optimal combination of several predefined augmentation strategies. Zoph *et al.* [58] deemed that borrowing off-the-shelf augmentation techniques of classification task contributes little to detection, thus they model the augmentation procedure as a discrete optimization problem and search for a best combination of preset augmentation operations. To this end, an efficient search technique based on reinforcement learning [59] was leveraged to explore for the optimal parameters. How-

ever, navigating such a large search space brings massive computations. To mitigate this situation, Cubuk *et al.* [60] optimized all of the operations jointly only with a single distortion magnitude while leaving the probability parameter uniform.

Most of the augmentation-based small object detection methods resort to increase the number of small instances to address the issue of data scarcity. Such data-level approaches, to a certain extent, could increase the positive samples and encourage the detector for better optimization on small objects. Nevertheless, they always suffer from the inconsistent performance improvement between datasets of different volumes and the poor transferability. In other words, the performance gain obtained by the manipulation-based methods is dataset-dependent.

2.3.2 Scale-aware methods

Objects in an image often vary in scale and such variation could be particularly severe in traffic scenarios and remote sensing images, leading disparate detection difficulties for a single detector. Previous approaches [61], [62] usually employ image pyramid [63] with sliding window scheme to handle the scale-variance issue. However, hand-crafted feature based methods, constrained by the limited representation capacity, perform catastrophically poorly on small objects. Early detection methods based on deep models still struggle in detecting tiny objects because only high-level features were used for recognition. To remedy the weakness of this paradigm and inspired by the success of reasoning across multi-level in other vision fields [64], [65], the following works mainly follow two paths. One refers to employ multi-scale features to detect the objects of various sizes in a divide-and-conquer fashion, and the other line of efforts intends to design tailored schemes for efficient training of multi-scale objects.

Multi-scale detection in a divide-and-conquer fashion.

The nature behind this line is simple: the features at different depths or levels were responsible for detecting the objects of corresponding scales only. HyperNet [66] supposes that the information of a Region of Interest (RoI) could distribute over all layers of backbone network and needs to be well organized. Based on this assumption, they concatenate and compress coarse-to-fine features to obtain Hyper Feature which retains the reasoning of small objects. Yang *et al.* [67] exploited scale-dependent pooling (SDP) to select a proper feature layer for subsequent pooling operation of small objects. MS-CNN [68] generates object proposals at different intermediate layers, each of which focuses on the objects within certain scale ranges, enabling the optimal receptive field for small objects. Liu *et al.* [49] devised Single Shot MultiBox Detector (SSD) to detect small objects on high-resolution feature maps. Following this roadmap, DSFD [69] employs two-shot detector connected by the feature enhancement module to detect the faces of various scales. YOLOv3 [45] conducts multi-scale predictions by adding parallel branches where high-resolution features are responsible for small objects. M2Det [70] constructs multi-level feature pyramids to detect objects.

In addition, combining scale-wise detectors for multi-scale detection has been extensively explored. Li *et al.* [71] built parallel subnetworks where small-size subnetwork is

learned specifically to detect small pedestrians. SSH [72] combines scale-variant face detectors, each trained for a certain scale range, to form a strong multi-scale detector to handle the faces varying extremely in scales. Trident-Net [73] builds a parallel multi-branch architecture where each branch possesses optimal receptive fields for the objects of different scales. Enlightened by the great success of region-level feature aggregation in PANet [74], Zhang *et al.* [75] concatenated the pooled features of an ROI at multiple depths with global feature to obtain more robust and discriminative representation for small traffic objects. QueryDet [76] designs the cascade query strategy to avoid the redundant computation on low-level features, making it possible to detect small objects on high-resolution feature maps efficiently.

Tailored training schemes. Based on the consensus that multi-scale training and testing could boost the prevailing deep detectors [73], [74], [77], the methods following this roadmap aim to develop customized data preparation strategies during training. Based on the generic multi-scale training scheme, Singh *et al.* [78] devised a novel training paradigm, Scale Normalization for Image Pyramids (SNIP), which only takes the instances whose resolutions fall into the desired scale range for training and the remainders are simply ignored. By this setting, small instances could be tackled at the most reasonable scales without compromising the detection performance on medium-to-large objects. Later, Sniper [79] advises to sample chips from a multi-scale image pyramid for efficient training. Najibi *et al.* [80] proposed a coarse-to-fine pipeline for detecting small objects. Considering that the collaboration between data preparation and model optimization is under-explored by previous methods [2], [63], [73], Chen *et al.* [81] designed a feedback-driven training paradigm to dynamically direct data preparation and further balance the training loss of small objects. Yu *et al.* [7] introduced a statistic-based match strategy for scale consistency.

Either multi-level representations or the specific training schemes strive for consistent performance gains of both small-scale objects and medium-to-large ones. However, divide-and-conquer paradigms map the objects of different sizes to corresponding scale levels may confuse detectors, because the information of single layer is inadequate to make accurate prediction. On the other hand, tailored mechanisms for boosting multi-scale training usually introduce extra computation, hindering the end-to-end optimization.

2.3.3 Feature-fusion methods

Deep CNN architecture produces hierarchical feature maps at different spatial resolutions, in which low-level features describe finer details along with more localization cues, while high-level features capture richer semantic information [13], [43], [73], [74], [82], [83]. Due to the existence of sub-sampling layers, the response of small objects may disappear at deeper layers. An alternative solution is to exploit the shallow features to detect small objects. Though conducive to localization, the feature maps at early stages are susceptible to variations such as illumination, deformation and object pose, making the classification task more challenging. To overcome this dilemma, extensive approaches leverage feature fusion, which integrates the features at

different layers or branches, to obtain better feature representation for small objects.

Top-down information interaction. Motivated by pyramidal architecture used in the era of hand-engineered features [63], seminal works [2], [84] construct top-down pathway to strengthen the interaction between shallow and deep layers, enabling that the high-resolution representations have rich semantics and fine localization of small objects simultaneously. Shrivastava *et al.* [84] introduced the Top-Down Modulation (TDM) network, where the top-down module learns what semantics or context should preserve and the lateral module transforms low-level features for subsequent fusion. Lin *et al.* [2] proposed Feature Pyramid Network (FPN), where early-stage features with high-resolution but low-level semantics are aggregated with late-stage features with low-resolution but high-level semantics. This simple yet effective design has become an essential component in feature extractor. To mitigate the deficiency of localization signals encountered in monodirectional pyramid architectures, PANet [74] enriches the feature hierarchy with bidirectional paths, enhancing deeper features with accurate localization signals. Zand *et al.* [85] constructed DarkNet-RI, on the basis of DarkNet-53 [44] and skip-connection [10], to generate high-level semantic feature maps at different scales.

Refined feature fusion. Despite its success and popularity, the basic interaction design is not perfect due to the inherent scale-level inconsistencies that basic up-sampling and fusion cannot deal with [74]. Observing this, the following approaches aim to refine the features emanated from different stages of the backbone trunk in a proper fashion [86], or optimize the fusion process by dynamically controlling the information flow between different layers [87], [88]. Woo *et al.* [86] proposed StairNet where deconvolution was exploited to enlarge the feature map, such learning-based up-sampling function can achieve a more refined feature than naïve kernel-based up-sampling and allows that the information of different pyramid levels propagates more efficiently [89]. Liu *et al.* [90] introduced IPG-Net, where a set of images at different resolutions obtained by the image pyramid [63] were input to the designed IPG transformation module to extract shallow features to complement spatial information and details. Gong *et al.* [87] devised a statistic-based fusion factor to control the information flow of adjacent layers. Noting that the gradient inconsistency encountered in FPN-based approaches deteriorates the representation ability of low-level features [91], SSPNet [88] highlights the features of specific scales at different layers and employs the relationship of adjacent layers in FPN to accomplish proper feature sharing.

Feature fusion approaches can bridge the spatial and semantic gaps between lower pyramidal levels and higher ones. However, small objects are usually assigned to the lowest pyramidal feature (highest spatial resolution) in current detection paradigms owing to the size-based pyramid assign strategy, which gives rise to the computational burden and redundant representations in practice. Moreover, in-network information flow is not always conducive to the representations of small objects. Our goal is to not only endow the low-level features with more semantics, but also prevent the original responses of small objects from

overwhelmed by deeper signals. Unfortunately, you cannot have your cake and eat it, hence this dilemma needs to be addressed carefully.

2.3.4 Super-resolution methods

One straightforward way to enrich the information of small objects is increasing the resolution of input images by bilinear interpolation [92] and super-resolution network [93]. Nevertheless, interpolation-based methods, as a local operation, usually fail to capture the global understanding and suffer from mosaic effect [94]. This situation will likely get worse for those objects with extremely limited sizes. Furthermore, we hope that the upscaling operation could restore the distorted structures of small objects instead of simply amplifying the ambiguous appearance of them. To this end, several tentative methods super-resolve input images or features by borrowing off-the-shelf techniques from super-resolution fields. Most of these approaches resort to Generative Adversarial Networks (GANs) [95] to compute high-quality representations which are conducive to small object detection, while others opt for parameterized upsampling operations to enlarge the features.

Learning-based upscaling. Blindly increasing the scale of input images incurs performance saturation [78] and non-negligible computational cost at feature extraction stage [96]. To overcome this difficulty, the methods following this line prefer to super-resolve the feature maps. They usually utilize learning-based upsampling operations to increase the resolution of feature maps and enrich the structures. On top of SSD [49], DSSD [89] employs deconvolution operation to obtain high-resolution features specialized for small object detection. Zhou *et al.* [82] and Deng *et al.* [96] explored sub-pixel convolution [97] for effective upsampling.

GAN-based super-resolution frameworks. Goodfellow *et al.* [95] proposed GAN to generate visually authentic data by following a two-player minimax game between the generator and the discriminator. Unsurprisingly, such capability enlightens the researchers to explore this powerful paradigm for generating high-quality representations of small objects. However, directly superresolving the whole images burdens the feature extractor in both training and inference. To mitigate this overhead, MTGAN [98] super-resolves the patches of RoIs with the generator network. Bai *et al.* [99] extended this paradigm to face detection task and Na *et al.* [100] applied super-resolution method to small candidate regions for better performance. Though super-resolving target patches could partly reconstruct the blurry appearance of small objects, this scheme neglects the contextual cues which play an important role for network prediction [101], [102]. To deal with this issue, Li *et al.* [103] devised PerceptualGAN to mine and exploit the intrinsic correlations between small-scale and large-scale objects, in which the generator learns to map the weak representations of small objects to super-resolved ones to deceive the discriminator. To go a step further, Noh *et al.* [101] introduced direct supervision to the super-resolution procedure.

Because of the limited size, the signals of small objects were unavoidably lost after feature extraction, leading the subsequent ROI pooling operation can barely compute structural representations. By mining the intrinsic correlations between small-scale objects and large-scale ones,

super-resolution frameworks allow for partly restoring the detailed representations of small objects. Nevertheless, either learning-based upscaling methods or GAN-based approaches have to maintain the balance between burdensome computation and the overall performance. Moreover, GAN-based methods are inclined to fabricate spurious textures and artifacts, imposing negative impacts on detection. Worse still, the existence of super-resolution architecture complicates the end-to-end optimization.

2.3.5 Context-modeling methods

We human can effectively utilize the relationship between the environment and the objects or the relation of objects to facilitate the recognition of objects and scenes [104], [105]. Such prior knowledge that captures the semantic or spatial associations is known as context, which conveys the evidence or cues beyond the object regions. The contextual information is of critical importance not only in visual systems of human [102], [104] but also in scene understanding tasks such as object recognition [106], semantic segmentation [107] and instance segmentation [108], *etc*. Interestingly, informative context sometimes can provide more decision support than the object itself, especially when it comes to recognizing objects with poor viewing quality [104]. To this end, several methods exploit the contextual cues to boost the detection of small objects.

Chen *et al.* [28] employed the representations of context regions which encompass the proposal patches for subsequent recognition. Hu *et al.* [92] investigated how to effectively encode the regions beyond the object extent and model the local context information in a scale-invariant manner to detect tiny faces. PyramidBox [105] makes full use of contextual cues to find small and blur faces that are indistinguishable from background. The intrinsic correlations of objects in an image can be regarded as context likewise. FS-SSD [109] exploits the implicit spatial context information, the distances between intra-class and inter-class instances, to redetect the objects with low confidence. Assuming that the original RoI pooling operation would break up the structures of small objects, SINet [110] introduces a context-aware RoI pooling layer to maintain the contextual information. IONet [111] computes global contextual features by two four-directional IRNN structures [112] for better detection of small and heavily occluded objects.

From the information theory perspective, the more types of features are considered, the more likely higher detection accuracy can be obtained [75]. Inspired by the consensus, context priming has been extensively studied to generate more discriminative features, especially for small objects who have inadequate cues, enabling precise recognition. Unfortunately, both holistic context modeling or local context priming confuse about which regions should be encoded as context. In other words, current context modeling mechanisms determine the contextual regions in a heuristic and empirical fashion, which cannot guarantee the constructed representations are interpretable enough for detection.

2.3.6 Others

The approaches belonging to the aforementioned five categories could cover the majority of the attempts that have

been made for boosting the small object detection, and we also replenish some other solutions and hope these strategies could inspire the readers to consider this challenging task from other interesting perspectives.

Attention-based methods. We human can quickly focus and distinguish objects while ignoring those unnecessary parts by a sequence of partial glimpses at the whole scene [118], [119], and this astonishing capacity in our perception system is generally referred as visual attention mechanism, which plays a crucial role in our visual system [120], [121]. Not surprisingly, this powerful mechanism has been extensively investigated in the previous literature [122], [123], [124], [125], [126] and shows great potential in many vision fields [5], [9], [127], [128]. By allocating different weights to different parts of feature maps, the attention modeling indeed emphasizes the valuable regions while suppressing those dispensable ones. Naturally, one can deploy this superior scheme to highlight the small objects that are inclined to be dominated by the background and noisy patterns in an image. Pang *et al.* [129] employed a global attention block to suppress the false alarms and efficiently detect small objects in large-scale remote sensing images. SCRDet [130] designs an oriented object detector, in which pixel attention and channel attention were trained in a supervised manner to highlight small object regions while eliminating the interference of noise. Extending the anchor-free detector FCOS [4] with the proposed level-based attention, FBR-Net [131] equilibrates the features at different pyramid levels and enhances the learning of small object under complicated situations.

Localization-driven optimization. Localization, as one of the primary tasks of detection, is formulated as a regression problem in most detection paradigms [1], [3], [4], [44], [45], [46], [47]. Nevertheless, the regression targets adopted in this ubiquitous branch of current detectors fail to reconcile with the evaluation metric, namely IoU. And this inconsistency of optimization will impair the performance of detectors, especially on tiny objects. Take this into consideration, several methods aim at equipping the localization branch with IoU-awareness or seeking for proper metrics. TinaFace [132] adds a DIoU [133] branch to RetinaNet [3] and ultimately acquires a simple but strong baseline for tiny face detection. Observing that IoU metric changes drastically due to the slight offsets of predicted boxes for tiny objects, Xu *et al.* [134] proposed a novel metric, Dot Distance, to alleviate this situation. Similarly, NWD [135] introduces the Normalized Wasserstein Distance to optimize the location metric for tiny object detectors.

Density analysis guided detection. Small objects in high-resolution images tend to distribute non-uniformly and sparsely [136], and the general divide-and-detect scheme consumes too much computation on those empty patches, leading the inefficiency during inference. Can we filter out those regions with no object thereby reducing the useless operations to boost the detection? The answer is YES! Efforts in this area break the chain of generic pipeline for processing high-resolution images, they first abstract the regions contain targets, on which the detection performs subsequently. Yang *et al.* [136] proposed a Clustered Detection network (ClusDet) that fully exploits the semantic and spatial information between objects to generate cluster chips

TABLE 2

Statistics of some benchmarks available for small object detection. ODNI stands for object detection in natural images and ODAI denotes object detection in aerial images. (1K = 1000, 1M = 1000K).

Dataset name	Task field	Publication	#Images	#Instances	Descriptions and Characteristics
COCO [6]	ODNI	ECCV 2014	123K	886K	One of the most popular datasets for generic object detection
SOD [28]	ODNI	ACCV 2016	4925	8393	A small-scale dataset for small object detection
WiderFace [8]	Face detection	CVPR 2016	32K	393K	A large-scale benchmark with rich annotations for face detection
EuroCity Persons [113]	Pedestrian detection	TPAMI 2019	47K	219K	The largest dataset for pedestrian detection captured from dozens of Europe cities
WiderPerson [114]	Pedestrian detection	TMM 2020	13K	39K	Pedestrian detection benchmark in traffic scenarios
TinyPerson [7]	Pedestrian detection	WACV 2020	1610	72K	The first dataset dedicated to tiny-scale pedestrian detection
TT100K [115]	Traffic sign detection	CVPR 2016	100K	30K	A realistic and large-scale benchmark for traffic sign detection
DIOR [20]	ODAI	JPRS 2020	23K	192K	One of the most frequently used benchmarks for object detection in aerial images
DOTA [30]	ODAI	TPAMI 2021	11K	1.79M	The largest remote sensing detection dataset including considerable small objects
AI-TOD [116]	ODAI	ICPR 2021	28K	700K	A tiny object detection dataset based on previous available datasets
NWPU-Crowd [117]	Crowd counting	TPAMI 2021	5109	2.13M	The largest dataset for crowd counting and localization to date

and then performs the detection. Following this paradigm, Duan *et al.* [57] and Li *et al.* [137] both exploited pixel-wise supervision to density estimation, achieving more accurate density maps which characterize the distribution of objects well.

Other issues. Several tentative strategies employ interesting techniques from other areas for better detection of small objects. Holding that traditional annotating fashion will introduce bias and ambiguity, Song *et al.* [138] suggested a novel topological annotation for pedestrians which allows more precise localization on small-scale instances with the proposed somatic topological line localization (TLL). Similar to super-resolution approaches, Wu *et al.* [139] employed the proposed Mimic loss to bridge the gap between the regional representations of small pedestrians and those of large-scale ones. Kim *et al.* [140], inspired by the memory process of human visual understanding mechanism, devised a novel framework for small-scale pedestrian detection based on the memory learning.

3 REVIEW OF DATASETS FOR SMALL OBJECT DETECTION

3.1 Datasets for Small Object Detection

Datasets are the cornerstone of learning-based object detection methods, especially for data-driven deep learning approaches. In the past decades, various research institutions have launched plenty of high-quality datasets [6], [30], [31], [32], and these publicly available benchmarks provide impartial platforms for validating the detection methods and significantly boost the development of related fields. Unfortunately, very few benchmarks are designed for small object detection. For the sake of integrity, we still retrospect a dozen datasets which contain considerable number of small objects, and expect to provide a comprehensive review of datasets. Instead of restricting our scope to specific tasks, we investigate the related datasets which span over a wide range of research areas, including face detection [8], pedestrian detection [7], [113], [114], object detection in aerial images [20], [30], [116], [141], to name a few. The statistics of these benchmarks are given in Tab. 2, and only the most representative among them were introduced below in detail due to the space restriction.

COCO. Pioneering works [31], [32], though push forward the development of vision recognition tasks, have been criticized for their ideal condition, where objects usually have large sizes and center on the images, bearing little resemblance to the real-world scenarios. To bridge this gap and foster fine level image understanding, COCO [6] was launched in 2014, its trainval set annotates 886K objects distributed in 123K images with instance-level mask, covering 80 common categories under complex everyday scenes. Comparing to previous datasets for object detection, COCO contains more small objects (about 30% instances in COCO trainset have an area less than 1024 pixels) and more densely packed instances, both of which challenge the detectors. Moreover, the fully segmented annotation and the reasonable evaluation metric encourage more accurate localization. All these features help COCO be the de facto standard for validating the effectiveness of object detection methods in past years.

WiderFace. WiderFace [8] is a large-scale benchmark towards accurate face detection, in which faces vary significantly in scale, pose, occlusion, expression, appearance and illumination. It contains 32203 images with a total of 393703 instances. Except common bounding box annotations, attributes including occlusion, pose and event categories were also provided, which allows thorough investigation for existing approaches. The faces in WiderFace are divided into three subsets, namely small (between 10-50 pixels), medium (between 50-300 pixels) and large (larger than 300 pixels), where small subset accounts for half of all instances.

TinyPerson. TinyPerson [7] focuses on the seaside pedestrian detection. TinyPerson annotates 72561 persons in 1610 images which are categorized into two subsets: tiny and small, according to their lengths. Due to the extremely tiny size, an ignore label was assigned to those regions that cannot be certainly recognized. As the first dataset dedicated to tiny-scale pedestrian detection, TinyPerson is a concrete step forward for tiny object detection. However, its limited number of instances and single pattern restrict its capacity to serve as a benchmark for SOD.

TT100K. TT100K [115] is a dataset for realistic traffic sign detection which includes 30000 traffic sign instances in 100000 images, covering 45 common Chinese traffic-sign classes. Each sign in TT100K is annotated with precise bounding box and instance-level mask. The images in

TABLE 3
Area subsets and corresponding area ranges of objects in SODA benchmark.

Area Subset	Tiny			Small
	extremely Tiny	relatively Tiny	generally Tiny	
Area Range	(0, 256]	(256, 576]	(576, 1024]	(1024, 2000]

TT100K are captured from Tencent Street Views, holding a high degree of variability in weather conditions and illuminance. Moreover, TT100K contains considerable small instances (80% of instances occupy less than 0.1% in the whole image area) and the entire dataset follows a long-tail distribution.

DOTA. DOTA [30] is proposed to facilitate the object detection in Earth Vision. It contains 18 common categories and 1793658 instances in 11268 images. Each object has been annotated with horizontal/oriented bounding box. Owing to the high diversity of orientations in overhead view images and large-scale variations among instances, DOTA dataset has numerous small objects, but they only distribute in a few categories (*small-vehicle*).

3.2 Evaluation metrics

Before diving into the evaluation criteria of small object detection, we first introduce related preliminary concepts. Given a ground-truth bounding box b_g and a predicted box b_p output by the detector, if the IoU between b_g and b_p is greater than the predefined threshold, and the predicted label is in accordance with the ground-truth, the current detected box will be identified as a potential prediction to this object, also known as True Positive (TP), otherwise it will be regarded as a False Positive (FP). Once we obtain the number of TP, FP and False Negative (FN, also known as missed positives), the Average Precision (AP) can be computed to evaluate the performance of detectors.

Average Precision. Average Precision (AP) is originally introduced in VOC2007 Challenge [31] and usually adopted in a category-wise manner. Concretely, given a confidence threshold and an IoU threshold β (0.5 for VOC2007), the Recall (R) and Precision (P) can be calculated afterwards. By varying the confidence threshold α , one can obtain different pairs (P, R) and ultimately, AP can be determined by averaging the precision scores under different recalls. This fixed IoU based AP metric once dominated the community for years.

A new evaluation metric was introduced with the launch of COCO dataset after 2014, which averages AP across multiple IoU thresholds between 0.5 and 0.95 (with an interval of 0.05). Apart from merely considering fixed IoU threshold, this criterion also takes the higher IoU thresholds into account, encouraging more accurate localization. This reasonable evaluation metric has been used as the “gold standard” in detection community and widely adopted by the following works [115], [142]. Noting that the overall AP is computed by averaging the APs of all categories in practice.

4 BENCHMARKS

In this section, we elucidate the data acquisition and annotation process for building SODA-D and SODA-A. Moreover,

we shed light on the characteristics of our benchmarks and the main differences among our datasets and related existing ones.

4.1 Data acquisition

Our aim is to build datasets tailored for small object detection, hence the point is **how to define a valuable object**.

Definition about a valuable object. Generally, a bounding box B can be represented as (x, y, w, h, θ) , where (x, y) denotes the center location and (w, h) indicates the width and height of the box respectively, the parameter θ stands for the orientation angle and is unused for horizontal annotation. Moreover, we use $S = w \times h$ to denote the pixel area of an object. Considering there is no distinct and unified definition about small objects, inspired by the previous works [6], [7], we adopt the absolute area criterion and regard an instance who has an area smaller than 2000 pixels, *i.e.*, $S \leq 2000$, as a valuable object, otherwise, the object comes to the *ignore* category and will not influence the final evaluation results. Intuitively, we can use the area ratio of an object to the image to define a small object, and the difference among these two definitions lies in that the latter relies on the image resolution, which could lead to a paradoxical situation: the objects with similar sizes appeared in two images with different resolutions will be categorized into two groups. Hence, we adopt the absolute area as the criterion to define a small object for the sake of consistency.

Empirically, 2000 is quite a loose bound for defining a small object, hence, as demonstrated in Tab. 3, we split the objects into two super-groups: *Tiny* and *Small*. In addition, considering the detection difficulty increases sharply when the object size gets smaller, we further divide the *Tiny* objects into three subsets: *extremely Tiny* (*eT*), *relatively Tiny* (*rT*) and *generally Tiny* (*gT*).

Scene Selection. To acquire a vast collection of small instances for training robust deep models, we carefully choose the driving scene and aerial scene to construct our datasets. Our prime motivations come as follow:

1. To capture size-limited objects, we need to increase the shooting distance, even so, the objects in the aforementioned two scenarios can still be identified due to their natural sizes and distributions. Moreover, the instances with similar sizes often occur intensively. This promises that we can obtain sufficient and valuable small instances.

2. The annotation types adopted in the two benchmarks are Horizontal Bounding Box (HBB) and Oriented Bounding Box (OBB), which actually correspond to two of the most fundamental detection tasks, horizontal object detection and oriented object detection. That is to say, our benchmarks are amenable for most of the SOD algorithms to conduct the evaluation and comparison.

3. These two scenes are both in high demand for SOD task: autonomous driving requires decision making based on the reliable and real-time understanding of complicated surroundings, where the objects far from the vehicle or occluded by other instances are with limited sizes, posing great challenges to the perception system. Meanwhile, overhead-view image analysis has an urgency to handle small objects in terms of the large flying altitude and various shooting views.

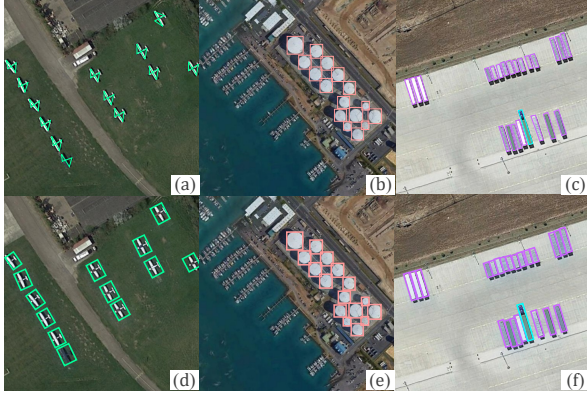


Fig. 3. Three types of annotations used in SODA-A, *i.e.*, crisscross polygon (a), horizontal bounding box (b) and enclosed polygon (c). The bottom (d, e, f) are the visualization results of oriented bounding boxes converted from original annotations.

Data source. The images in SODA-D are mainly from MVD [33], self-shooting and the Internet. MVD is a large-scale dataset for semantic understanding of street scenes, of which 25000 high-quality images are captured from road views, highways, rural areas and off-road. Thanks to the high-quality and high-resolution property with MVD, we can obtain a large set of valuable instances with clear visual structure. For self-shooting part, we use on-board cameras and mobile phones to collect images of typical driving scenes in several Chinese cities, including Beijing, Shenzhen, Shanghai, Xi'an, Qingdao, Guangzhou, *etc.* In addition, we also crawl images by searching keywords on the image search engines (Google, Bing, Baidu, *etc.*). Finally, we obtained 30126 raw images of traffic scene.

Enlightened by the pioneering works [20], [30], Google Earth² was leveraged to collect images for SODA-A, we extract 2976 images from hundreds of cities around the world suggested by the experts. It is noting that numerous images with cluttered background and high density which are closer to realistic challenges are captured. In addition, the images in SODA-A have a relatively high resolution and most of them enjoy a resolution larger than 4700×2700 , enabling the finer details and adequate context that are of great significance to small object detection [104], [105].

Data Cleaning. For SODA-D, the images that are visibly affected by artifacts, lens flare, strong motion blur and other factors which impede the subsequent annotation process were removed. Moreover, duplicated images collected from different websites were cleaned either. For SODA-A, we eliminate those images with noticeable blur and artifacts. After cleaning, we finally obtain 24704 and 2510 valid images for SODA-D and SODA-A respectively.

Dataset split. Following the pioneering works [6], [33], we split the full image-set into three subsets: train-set, validation-set and test-set, and each subset occupies 50%, 20% and 30% approximately.

License declaration. Our two benchmarks are freely available under the CC-BY-SA license agreement³.

TABLE 4
Numbers of instances of each category and three splits of SODA-D (Left) and SODA-A (Right).

Category	#Instances	Category	#Instances
people	35907	airplane	31529
rider	4600	helicopter	1395
bicycle	2524	small-vehicle	463072
motor	3839	large-vehicle	15333
vehicle	69125	ship	61916
traffic-sign	85896	container	138223
traffic-light	62282	storage-tank	35027
traffic-camera	7525	swimming-pool	26953
warning-cone	5898	windmill	26755
Train	134301	Train	344228
Validation	55213	Validation	159573
Test	88082	Test	296402
Total	277596	Total	800203

4.2 Data annotation

Annotation tools. As we alluded to before, the annotation type for the two benchmarks is different. Specifically, we annotate the objects of SODA-D with horizontal bounding boxes, and the instances of SODA-A are annotated with polygons which is in line with the pioneering works [20], [30]. To precisely and efficiently annotate the instances with limited sizes in our database, we use Labelimg⁴ and Labelme⁵ toolkits to conduct the annotations of SODA-D and SODA-A, which both allow for high-degree zoom-in operation, enabling the fine-grained annotations.

Category selection. Take the realistic value for applications and the intrinsic size into consideration, we select 9 valuable categories for SODA-D: *people*, *rider*, *bicycle*, *motor*, *vehicle*, *traffic-sign*, *traffic-light*, *traffic-camera*, and *warning-cone*. For SODA-A, we also annotate 9 object classes: *airplane*, *helicopter*, *small-vehicle*, *large-vehicle*, *ship*, *container*, *storage-tank*, *swimming-pool*, and *windmill*.

Box-level annotation. The annotation of SODA-D resembles that of general detection benchmarks [6], [31], [32]: drawing tight bounding box enclosing the target, hence we put the emphasis on describing our annotation of SODA-A. To efficiently perform the labeling process, we tailor optimal annotation strategies for different categories. For *airplane* and *helicopter* category, we design a new type of annotation method, crisscross annotation, which only requires four extreme points and is more appropriate to the objects with cruciform structures. In addition, we simply adopt horizontal box for *storage-tank* and *windmill* category. For remaining classes, the annotators use Labelme toolkit to create enclosed polygons along the contours of instances. Finally, the post-processing code was employed to convert the above annotations to unified oriented bounding box annotations. The visualization of the three types of annotations and converted oriented bounding boxes are shown in Fig. 3.

For the ignored regions of images in the two datasets, the general principle during annotation is merging these areas as possible while avoiding surround valuable foreground instances. This preliminary annotation stage of the two benchmarks costs about 6150 hours in total, and involves 16 well-trained annotators.

2. <https://earth.google.com/>

3. <https://creativecommons.org/licenses/by-nc/4.0/>

4. <https://github.com/tzutalin/labelImg>

5. <https://github.com/wkentaro/labelme>

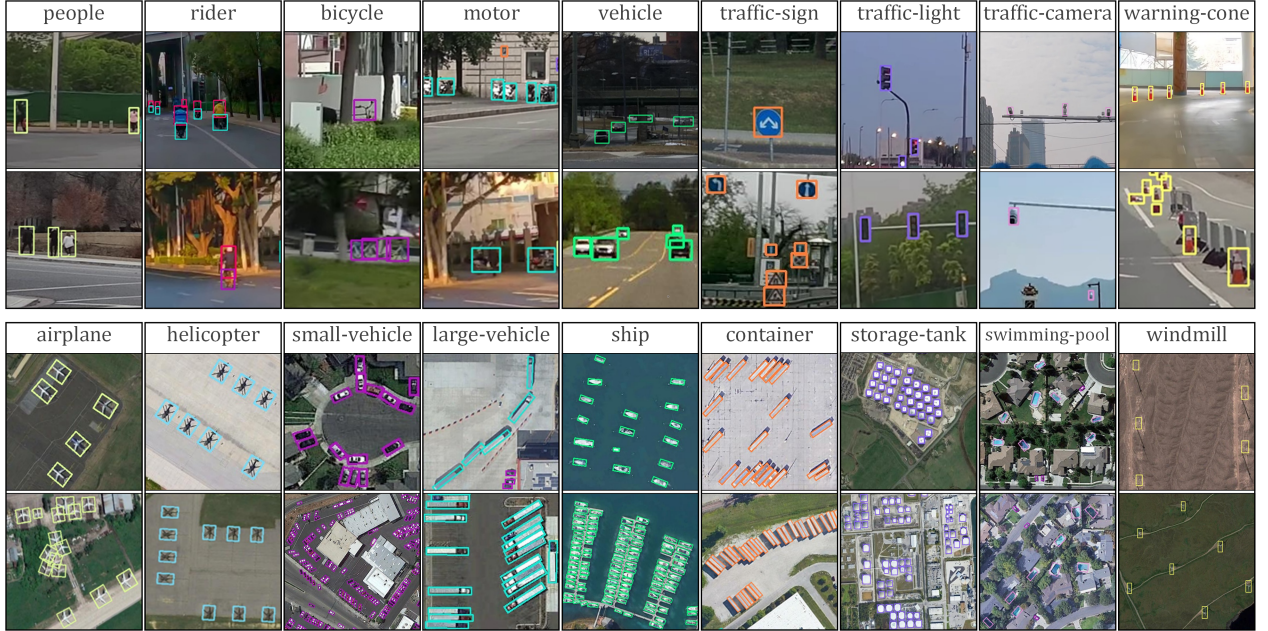


Fig. 4. Example instances of each category in SODA-D (Top) and SODA-A (Bottom).

TABLE 5

Comparisons between SODA-D and several related detection datasets under driving scene (Top), likewise for SODA-A and some detection datasets under aerial scenario (Bottom). Note that eT , rT and gT stand for *extremely Tiny*, *relatively Tiny* and *generally Tiny* according to our definition (see Tab. 3). And for each dataset, we only count the subsets whose annotations are available, see Split column. Avg. Res. denotes the average image resolution of the dataset. HBB/OBB denotes horizontal/oriented bounding box.

Dataset	#Images	#Categories	#Instances			Split	Avg. Res. (W × H)	Year
			eT	rT	gT			
TT100K [115]	8876	45	729	4584	3988	train/test	2048 × 2048	2016
EuroCity Persons [113]	32605	18	16588	36070	38548	train/val	1920 × 1024	2019
TJU-DHD Traffic [142]	50266	5	82	4088	17385	train/val	1624 × 1200	2021
SODA-10M [143]	10000	6	886	5278	6986	train/val	1920 × 1080	2021
SODA-D	24704	9	58522	74253	64692	train/val/test	3407 × 2470	2022

Dataset	Annotation	#Images	#Categories	#Instances			Split	Avg. Res. (W × H)	Year
				eT	rT	gT			
CARPK [144]	HBB	1448	1	47	512	1378	train/test	1280 × 720	2017
VisDrone [145]	HBB	8629	10	128964	90107	65972	train/val/test-dev	1490 × 957	2021
AI-TOD [116]	HBB	28036	8	301753	35729	8484	train/val	800 × 800	2021
DOTA [30]	OBB	2423	18	181124	52583	45139	train/val	2217 × 2074	2021
DIOR-R [141]	OBB	23463	20	50059	34443	23604	train/val/test	800 × 800	2022
SODA-A	OBB	2510	9	491891	161966	110744	train/val/test	4761 × 2777	2022

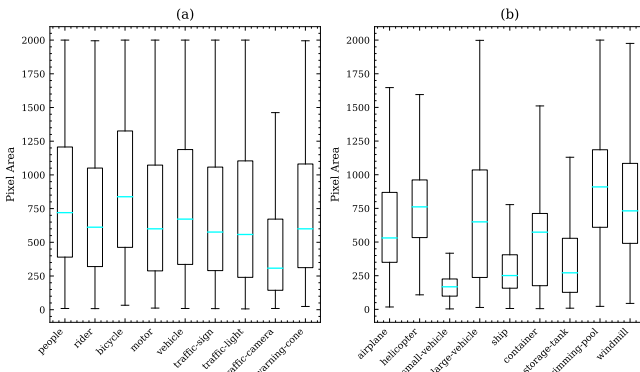


Fig. 5. Category-wise area distribution of instances in SODA-D (a) and SODA-A (b).

Quality assurance. As stated in [146], [147], the annotation quality of a dataset is the dominating factor for its lifespan as a benchmark, hence we install a two-step quality assurance procedure after the initial annotation. Concretely, at first step, each of the 16 professional annotators is respon-

sible for reviewing the annotations of others and reporting back the existing problems to the original annotator to minimize missing or incorrect labeling. In order to further improve the final quality, 8 senior inspectors are divided into two groups to conduct second-step verification. Each image was revisited by four assessors, and it will be put back into the pool to relabel if two or more experts are skeptical of the annotation. This process will not end until there is no images left in the pool. After careful verification, the overall annotation quality can be ensured. This assurance phase spends about 880 hours.

4.3 Statistical analysis

We annotate 277596 instances for SODA-D and 800203 objects for SODA-A, the number of instances for each category and that for three subsets are shown in Tab. 4. Also the instances of each category are shown in Fig. 4. From Tab. 5, SODA-D and SODA-A both far exceed the existing mainstream object detection datasets under traffic



Fig. 6. Example images under diversified conditions in our SODA-D dataset, where masked bounding boxes represent *ignore* regions. Best viewed in zoom-in windows.

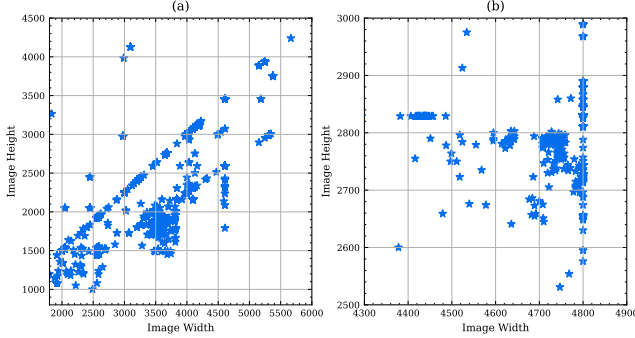


Fig. 7. The distribution of image resolution in SODA-D (a) and SODA-A (b). Note that we randomly sample 2000 images to obtain the size profile for clear illustration.

and aerial scenarios on the amount of *Tiny* objects, especially for *extremely Tiny* ones. Moreover, we also show the category-wise instance area distribution of SODA-D and SODA-A in Fig. 5. As can be seen, the area of objects in our benchmarks falls into a relatively tight range. Except the data volume, our SODA-D and SODA-A also exhibit several unique characters, as discussed next.

4.3.1 Data properties of SODA-D

Rich diversity. Our SODA-D dataset inherits one of the most preeminent virtues of MVD: rich diversity in terms of locations, weathers, period, shooting views and scenarios. Fig. 6 shows some examples of our dataset covering various weather, view and illumination conditions. We believe that our diverse data could empower the model with the ability to generalize to different situations.

High spatial resolution. The images in SODA-D enjoy very high resolution and high quality, which is entailed for small or tiny object detection. In Fig. 7, we demonstrate the distribution of image resolution in SODA-D, and the average resolution at 3407×2470 shows a clear predominance in comparison with previous datasets who focus on object detection under traffic scenes, as illustrated in Tab. 5.

Ignore regions. Albeit we carefully select images for SODA-D, there still exists some areas to be ignored for

evaluation stability, as done in previous works [7], [8], [148]. Concretely, we assign *ignore* label to: 1) the instances belonging to the preset categories but with an area greater than 2000; 2) the objects that are excessively small and heavily occluded thus cannot be distinguished. We deem that the prevailing detectors [1], [3], [4], [5], [9], [45], [47], [50], [51], [52], [149] can handle the first situation well, hence it is not our concern. For the latter condition, our well-trained annotators are called for cautiously labeling the regions as *ignore*, when they cannot make confident judgment even at highest zoom-in level, and it will only bring error and instability if we insist on annotating these regions as foreground objects. To put it in another way, *can we expect current algorithms to outperform human's eyes?* Therefore, categorizing these regions into *ignore* will not impose negative impact during evaluation process, and can guarantee the models concentrate on the authentic and valuable small objects.

4.3.2 Data properties of SODA-A

We show an example image of SODA-A in Fig. 8 and the local zoom-in windows exhibit the details of annotated instances.

Large density variation. As demonstrated in Fig. 9, the number of instances per image in SODA-A varies significantly from 1 to 11134, which implies that our benchmark not only contains sparse condition but also includes numerous images where the objects positioned in extremely close proximity. Moreover, the average number of instances per image in SODA-A is 318.81, which is twice the number of DOTA (159.18). Such distribution literally calls for a robust model with the capacity of handling excessively clustered situation.

Various orientations. The instances in SODA-A can appear in an arbitrary-rotated fashion. We indicate the orientation distribution of SODA-A in Fig. 9, and the tilt angle of annotated instances distributes from $-\pi/2$ to $\pi/2$. Note that we do not follow the orientation definition in DOTA, because most objects with tiny size cannot convey sufficient visual cues to determine their head or tail.

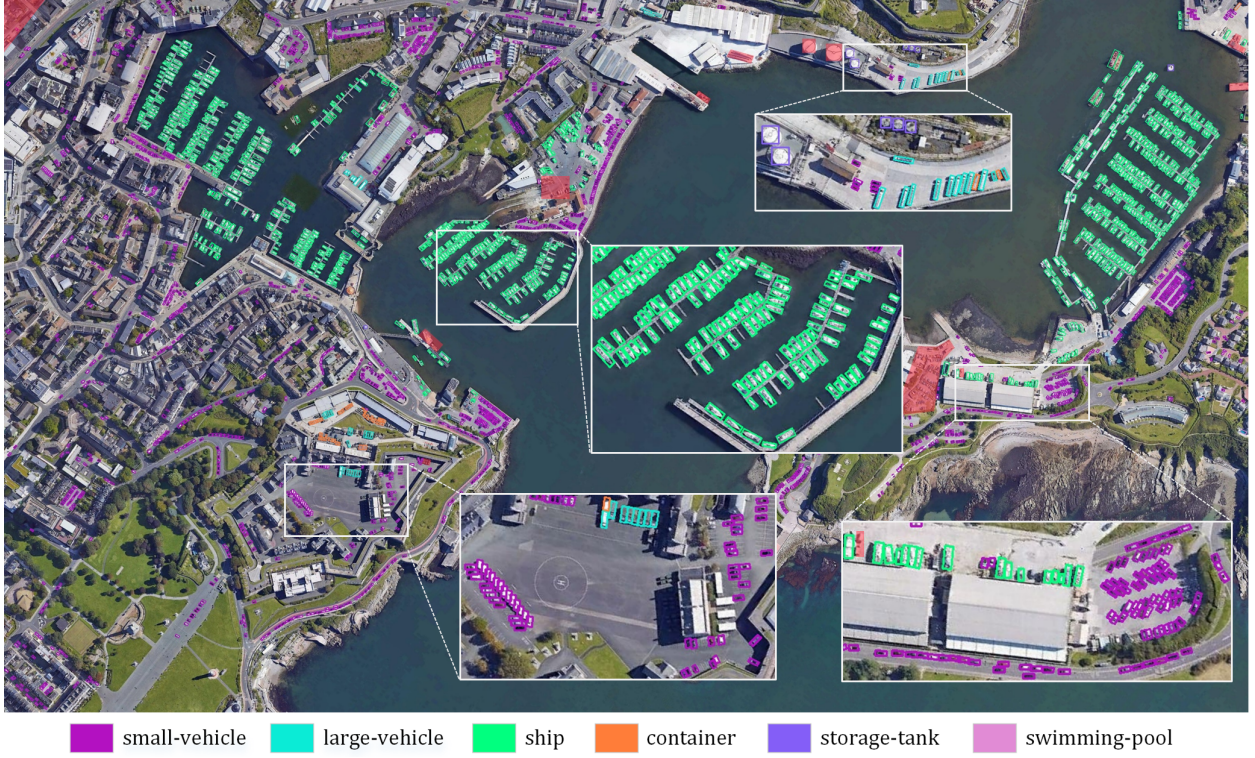


Fig. 8. An example image in SODA-A, the instances of different categories are best viewed in color and zoom-in windows, where masked areas denote the *ignore* regions.

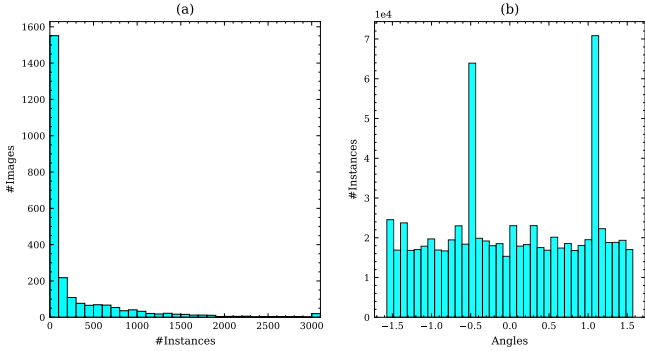


Fig. 9. Density distribution per image (a) and the orientation profile (b) of instances in SODA-A. Note that the number of images with more than 3000 instances were accumulated for clear demonstration of (a).

Diverse locations. The images in SODA-A are collected from hundreds of cities around the world, which substantially enhances the data diversity in fact (*e.g.*, the appearance of *airplane* objects in our SODA-A can vary considerably). Furthermore, the concomitant intra-class variation and complicated background bring more challenges.

4.4 Comparisons with previous benchmarks

Although there have been tremendous datasets for object detection, few of them dedicated to SOD task. Even so, we compare several related benchmarks with SODA to highlight its uniqueness.

4.4.1 SODA-D

MVD: Despite the SODA-D dataset is constructed on top of MVD, our intention is completely different from MVD. To be more specific, MVD concentrates on the pixel-level understanding of street scenes, while the proposed SODA-D highlights the detection of those objects with extremely small size under complicated driving scenarios.

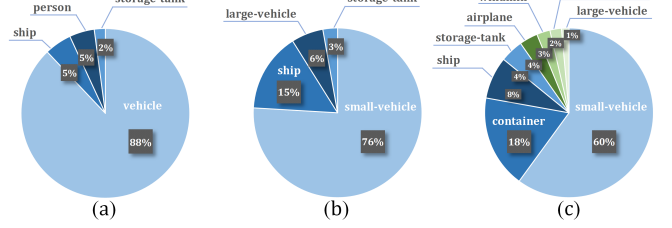


Fig. 10. Class distribution of *Tiny* instances in AI-TOD (a), DOTA (b) and SODA-A (c). Those categories with instances less than 2000 are not included.

4.4.2 SODA-A

AI-TOD: AI-TOD is built on several publicly available datasets, including DIOR [20], DOTA [30], VisDrone [145], xView [150], and Airbus-Ship⁶. However, the above datasets were not designed for SOD task, hence more than 88% instances of AI-TOD come from the category *vehicle*, leading to a non-negligible imbalance issue as shown in Fig. 10. Meanwhile, each category in our SODA-A contains adequate instances, except *helicopter* class, and this advantage becomes more pronounced when considering the data volume (our SODA-A contains 764601 instances belonging to *Tiny* object subset). In addition, the images in AI-TOD are cropped from existing datasets and the image resolution is fixed to 800×800 . More importantly, AI-TOD only provides horizontal annotations, which severely limits its capacity to approach objects accurately and to handle the densely-packed situation that is common and challenging for SOD in aerial images. In contrast, from Tab. 5 and Fig. 7, our SODA-A possesses an average image resolution of 4761×2777 , and the well-annotated oriented boxes allow for large density cases and encourage more accurate localization.

6. <https://www.kaggle.com/c/airbus-ship-detection>

TABLE 6

Baseline results on SODA-D test-set. All the models are trained with a ResNet-50 as the backbone. Schedule denotes the epoch setting during training, where '1×' refers to 12 epochs and '50e' represents 50 epochs.

Method	Publication	Schedule	AP	AP ₅₀	AP ₇₅	AP _T	AP _{eT}	AP _{rT}	AP _{gT}	AP _S
Faster RCNN [1]	TPAMI 2017	1×	32.9	64.5	29.4	28.9	19.3	30.1	35.8	43.2
Cascade RCNN [149]	TPAMI 2021	1×	35.7	64.6	33.8	31.2	20.4	32.5	39.0	46.9
RetianNet [3]	TPAMI 2020	1×	29.2	58.0	25.3	25.0	15.7	26.3	31.8	39.6
FCOS [4]	TPAMI 2022	1×	28.7	55.1	26.0	23.9	11.9	25.6	32.8	40.9
RepPoints [151]	ICCV 2019	1×	32.9	60.8	30.9	28.0	16.2	29.6	36.8	45.3
ATSS [152]	CVPR 2020	1×	30.1	59.5	26.3	26.1	17.0	27.4	32.8	40.5
Deformable-DETR [52]	ICLR 2020	50e	23.4	50.6	18.8	19.2	10.1	20.0	26.5	34.2
Sparse RCNN [153]	CVPR 2021	1×	28.3	55.8	25.5	24.2	14.1	25.5	31.7	39.4

TABLE 7

Category-wise AP of baseline detectors on SODA-D test-set. The training settings are consistent with Tab. 6 and the full names of class abbreviation are as follows: t-sign (traffic-sign), t-light (traffic-light), t-camera (traffic-camera) and w-cone (warning-cone).

Method	people	rider	bicycle	motor	vehicle	t-sign	t-light	t-camera	w-cone	AP
Faster RCNN [1]	41.3	20.1	17.8	25.7	50.3	49.9	41.8	15.9	33.3	32.9
Cascade RCNN [149]	45.5	21.8	21.1	27.1	54.1	52.8	44.7	16.7	37.3	35.7
RetianNet [3]	36.7	15.1	12.1	20.1	47.9	48.3	39.0	13.8	29.3	29.2
FCOS [4]	36.5	16.3	14.9	22.7	48.0	44.1	37.3	11.4	27.3	28.7
RepPoints [151]	42.9	19.7	16.1	24.4	52.5	51.2	42.6	14.5	32.6	32.9
ATSS [152]	37.8	18.0	15.3	22.9	48.2	47.1	38.5	12.9	30.2	30.1
Deformable-DETR [52]	30.0	12.5	10.6	17.7	37.3	39.7	30.3	9.0	24.0	23.4
Sparse RCNN [153]	38.1	15.5	11.6	21.3	46.4	46.9	37.8	10.1	27.2	28.3

TABLE 8

The AP performance of baseline detectors with different backbone networks. All the models were trained for '1×' schedule.

Method	ResNet-50	ResNet-101	Swin-T
Faster RCNN [1]	32.9	33.1	34.5
Cascade RCNN [149]	35.7	35.3	37.4
RetianNet [3]	29.2	29.6	33.1
FCOS [4]	28.7	29.2	34.0
RepPoints [151]	32.9	33.2	33.3
ATSS [152]	30.1	30.3	30.2
Sparse RCNN [153]	28.3	29.8	28.7

DOTA: DOTA is the largest dataset for object detection in aerial images to date. Compared to DOTA, who puts emphasis on scale variation issue, we mainly focus on the tiny-scale objects which obstruct current detectors. Moreover, though DOTA contains substantial amounts of small objects, most of them centralized at *small-vehicle*, as in Fig. 10.

5 EXPERIMENTS

5.1 Evaluation Protocol

Following the evaluation protocols in COCO [6], we use the Average Precision (AP) to evaluate the performance of detectors. Concretely, as the paramount metric, the overall AP is obtained by averaging the AP over 10 IoU thresholds between 0.5 and 0.95 (with an interval of 0.05). AP₅₀ and AP₇₅ are computed at the single IoU thresholds of 0.5 and 0.75, respectively. Moreover, we report the AP of *Tiny* category, *i.e.*, AP_T, to highlight our concern for tiny objects, and the AP of four area subsets also are demonstrated, namely, AP_{eT}, AP_{rT}, AP_{gT} and AP_S.

5.2 Implementation Details

To conduct fair comparisons of several benchmarking baselines, all the experiments on SODA-D and SODA-A are

implemented on top of the open source object detection toolbox mmdetection⁷ [154] and mmrotate⁸ [155], respectively. Directly feeding the high-resolution images in SODA to deep model is infeasible due to the GPU memory limitation, hence we crop original images into a series of 800 × 800 patches with a stride of 650. These patches will be resized to 1200 × 1200 during training and testing, which could partly alleviate the information loss caused in the feature extraction stage. Noting the patch-wise detection results will be first mapped to the original images, on which Non Maximum Suppression (NMS) was performed to prune out redundant predictions. We use 4 NVIDIA GeForce RTX 3090 GPUs to train the models, the batch size is set to 8 for the experiments of SODA-D and 4 for that of SODA-A, where the angle ranges is $[-\pi/2, \pi/2]$. During training, '1×' schedule (a budget of 12 epochs) was adopted except for Deformable DETR [52], which was trained for 50 epochs. Only random flip was used for augmentation. For all experiments, FPN [2] was employed to capture hierarchical and detailed representations for better performance. Detailed settings and hyperparameters please refer to our code library.

5.3 Results Analysis on SODA-D

In this section, we perform a rigorous evaluation of several representative methods on our SODA-D dataset, and provide in-depth analyses on top of the results.

5.3.1 Benchmarking Results

Tab. 6 reports the results of 8 representative methods on SODA-D test-set. From the table, we find that the Cascade RCNN [149] attains the best performance with an AP of 35.7% and AP_T of 31.2%, both of which steadily outperform

7. <https://github.com/open-mmlab/mmdetection>

8. <https://github.com/open-mmlab/mmrotate>

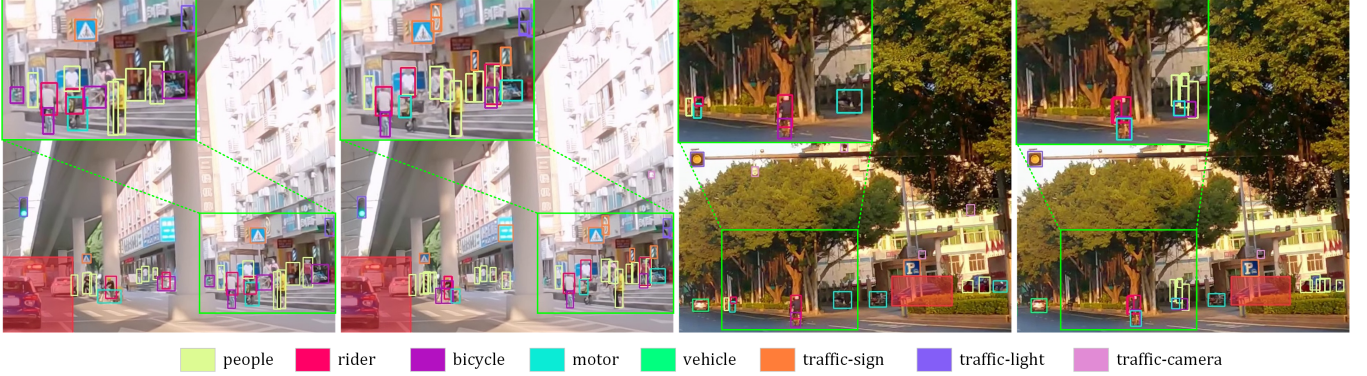


Fig. 11. Qualitative results of Cascade RCNN [149] on SODA-D test-set. Columns 1 and 3 denote the ground-truth annotations and columns 2 and 4 stand for the predictions. Best viewed in color and zoom-in windows, where masked bounding boxes represent *ignore* regions. Only predictions with confidence scores larger than 0.3 are demonstrated.

other detectors. Benefiting from the cascade structure, Cascade RCNN obtains an impressive AP_{75} of 33.8%, showing dominance in accurate detection of small objects. After that, Faster RCNN [1] and RepPoints [151] tie for the second place in ranking with an overall AP of 32.9%. More interestingly, if we delve into the specific metrics, Faster RCNN could surpass RepPoints by 0.9 points on AP_T score, and for the smallest area category, *i.e.*, *extremely Tiny*, the performance disparity comes to staggering 3.1 points. This phenomenon indicates that point representation, in comparison to its box counterpart, may not be a good choice for tiny objects, but show great potential for large ones. Moreover, RepPoints performs better on accurate localization, it can achieve an impressive AP_{75} score than Faster RCNN (30.9% *vs.* 29.4%). One-stage detector RetinaNet [3] scores 29.2% and 25.0% on AP and AP_{75} metrics respectively, which are largely inferior to the two-stage Faster RCNN. We conjecture this dense sampling fashion is unamiable to small objects who only occupy a relatively small area, thereby exacerbating the foreground-background imbalance problem. As for anchor-free detectors, ATSS [152] can achieve 30.1% AP and 26.1% AP_T on our SODA-D test-set, which are superior to the center-based method FCOS [4] (28.7% AP and 23.9% AP_T), and the latter behaves badly on *extremely Tiny* objects. This may partly originates from the occlusion challenge of our dataset, also known as the ambiguous sample problem. For the query-based detector, Sparse RCNN [153] achieves 28.3% AP and 24.2% AP_T , which are comparable to FCOS. Though exploiting multi-scale deformable attention to reduce high computation in encoder and enabling the access of high-resolution features, Deformable DETR [52] only delivers 23.4% AP and 19.2% AP_T , lagging noticeably behind other competitors even with more training epochs. This performance gap reveals that the sparse query paradigm could not cover small objects adequately, and the low recall rate further substantiates this⁹.

5.3.2 Category-Wise Results

We also list the category-wise results on Tab. 7, from which we can see that the AP of *rider*, *bicycle*, *motor* and *traffic-camera* are clearly inferior to other categories, we deem that the root cause of this phenomenon comes from two

9. Constrained by the space, the elaborate experiment results will be released on our homepage (<https://shaunyuan22.github.io/SODA>).

fold. 1) Class-imbalance issue, these categories contain less samples compared to other classes, *e.g.*, only 2524 samples included in *bicycle* category. 2) The limited area, for instance, nearly half of the *traffic-camera* objects possess an area less than 256 pixels, as demonstrated in Fig. 10. In other words, this phenomenon corroborates previous findings, *i.e.*, the detection difficulty increases sharply when the object size gets smaller.

5.3.3 Baseline Detectors with Different Backbones

Tab. 8 shows the performance of baseline detectors with different backbone networks. Compared to ResNet-50, ResNet-101 only brings a slight improvement even degrades the performance (see Cascade RCNN and Sparse RCNN). Concretely, such performance gain actually originates from the enhanced capability of detectors for handling those *Small* objects, in other words, the detection accuracy on *Tiny* objects drops instead. This phenomenon substantiates previous hypothesis that deeper models might not be better for the size-limited objects and moreover, the highly structural representations in deeper layers which hardly contain small object cues are suboptimal for detection. Swin-T [156] yields substantial improvements for almost all the detectors, especially for RetinaNet (+3.9 points) and FCOS (+5.3 points). This impressive performance reveals the powerful representation ability of shifted-window scheme for small objects, and could shed more light on the subsequent feature extractor design of SOD.

5.3.4 Qualitative Results

Fig. 11 demonstrates the visualization results of Cascade RCNN on SODA-D test-set. The first pair shows the challenge under complicated background and heavy occlusion, where the detector can hardly learn discriminative representation from instances with limited sizes and is inclined to lose those instances resembled the background. In addition, identifying those partly occluded objects is even more challenging. The second pair represents the detections of low illumination, in which the detector fails to recognize those instances under the shadow, still less predicts accurate bounding boxes.

5.4 Results Analysis on SODA-A

Based on SODA-A, we investigate the performance of several leading methods of oriented object detection.

TABLE 9

Baseline results on SODA-A test-set. All the models are trained with a ResNet-50 as the backbone. Schedule denotes the epoch setting during training, where ‘1×’ refers to 12 epochs.

Method	Publication	Schedule	AP	AP ₅₀	AP ₇₅	AP _T	AP _{eT}	AP _{rT}	AP _{gT}	AP _S
Rotated Faster RCNN [1]	TPAMI 2017	1×	34.0	72.6	25.7	32.5	18.6	34.2	39.0	34.4
Rotated RetinaNet [3]	TPAMI 2020	1×	28.1	66.1	17.4	26.8	14.9	28.3	32.8	28.2
RoI Transformer [157]	CVPR 2019	1×	37.7	75.5	32.1	36.0	20.7	37.3	43.3	39.5
Gliding Vertex [158]	TPAMI 2021	1×	33.2	73.2	24.1	31.7	18.6	32.6	38.6	33.8
Oriented RCNN [159]	ICCV 2021	1×	36.0	73.2	30.4	34.4	19.5	35.6	41.2	36.7
S ² A-Net [160]	TGRS 2022	1×	29.6	72.4	14.0	28.3	15.6	29.1	33.8	29.5
DODet [161]	TGRS 2022	1×	32.4	69.5	24.4	30.9	17.7	32.0	36.6	32.9

TABLE 10

Category-wise AP of baseline detectors on SODA-A test-set. The training settings are consistent with Tab. 9 and the full names of class abbreviation are as follows: s-vehicle (small-vehicle), l-vehicle (large-vehicle), s-tank (storage-tank) and s-pool (swimming-pool).

Method	airplane	helicopter	s-vehicle	l-vehicle	ship	container	s-tank	s-pool	windmill	AP
Rotated Faster RCNN [1]	50.5	18.2	33.3	24.5	43.5	29.9	43.8	37.0	25.0	34.0
Rotated RetinaNet [3]	42.3	16.6	30.1	14.1	35.6	23.1	35.8	34.3	20.6	28.1
RoI Transformer [157]	54.2	21.7	26.1	31.7	46.5	35.7	45.7	40.8	26.7	37.7
Gliding Vertex [158]	48.1	12.4	33.3	26.9	43.4	29.8	44.3	34.8	25.7	33.2
Oriented RCNN [159]	52.8	19.8	34.3	30.9	45.1	32.0	44.0	40.0	25.3	36.0
S ² A-Net [160]	42.1	19.8	31.2	18.8	36.8	26.1	30.4	37.5	24.2	29.6
DODet [161]	50.3	19.4	31.3	19.9	40.3	24.1	43.3	38.1	24.8	32.4

TABLE 11

The AP performance of baseline detectors on SODA-A test-set with different backbone networks. All the models were trained for ‘1×’ schedule.

Method	ResNet-50	ResNet-101	Swin-T
Rotated Faster RCNN [1]	34.0	34.3	35.2
Rotated RetinaNet [3]	28.1	28.1	24.3
RoI Transformer [157]	37.7	37.6	37.8
Gliding Vertex [158]	33.2	33.5	34.5
Oriented RCNN [159]	36.0	36.2	36.8
S ² A-Net [160]	29.6	29.7	27.1

5.4.1 Benchmarking Results

Tab. 9 shows the results of 7 representative methods on SODA-A test-set. RoI Transformer [157] achieves top performance with 37.7% AP and 36.0% AP_T. This remarkable success can be attributed to its powerful proposal generator, in which rotated proposals produced by the RRoI Learner can guarantee the high recall of small objects. By revising vanilla Faster RCNN to output an additional angle prediction, Rotated Faster RCNN [1] scores 34.0% and 32.5% on AP and AP_T respectively. This validates the robustness of this prevailing method again. Oriented RCNN [159] obtains a relatively high performance both at overall AP (36.0%) and AP_T (34.4%). Thanks to its efficient oriented RPN, Oriented RCNN can generate high-quality proposals with negligible parameter grow. From the results of RoI Transformer and Oriented RCNN, we can see that high-quality proposals are of great significance to small object detection, particularly for the densely packed objects. Gliding Vertex [158] and DODet [161] both resort to novel representations for oriented objects, the former learns four gliding offsets to corresponding sides while the latter utilizes aspect ratio and area to denote an object. Gliding Vertex achieves 33.2% and 31.7% on AP and AP_T slightly ahead of DODet (32.4% and 30.9%), however DODet performs better on AP₇₅ metric. For one-stage detectors, Rotated RetinaNet [3] achieves 28.1% AP and 26.8% AP_T respectively, we deem that in addition to the imbalance issue of foreground-background, it suffers from the misalignment between proposals and object features with limited size, exacerbating the

TABLE 12

AP vs. Speed of Oriented RCNN [159] with different number of proposals per patch on SODA-A test-set. FPS is tested on a single RTX 2080Ti GPU.

Proposal Num	1000	2000	3000	4000	5000	6000	7000	8000
AP	35.5	36.0	36.2	36.1	36.0	36.2	35.8	35.9
AP _T	33.9	34.4	34.5	34.4	34.4	34.6	34.2	34.1
Speed (FPS)	13.3	12.3	11.0	10.5	9.9	9.4	9.1	8.7

subsequent classification task. S²A-Net [160] designs feature alignment module to alleviate the misalignment problem, and finally achieves an AP with 29.6% and AP_T with 28.3%. Though it can substantially increase the score of AP₅₀, the concomitant performance decline on the AP₇₅ metric can be non-negligible (-3.4 points) when compared to Rotated RetinaNet, which indicates that the performance gain of S²A-Net is likely to come at the cost of subsequent regression accuracy.

5.4.2 Category-Wise Results

Category-wise results of baseline algorithms on SODA-A test-set are shown in Tab. 10. The AP of *helicopter* category is observably below that of other classes due to limited instance numbers. Moreover, the objects of *large-vehicle* and *container* with elongated structure challenge the regression branch, which can be confirmed in subsequent visualization results. Interestingly, top detector RoI Transformer achieves the lowest score on *small-vehicle* category.

5.4.3 Baseline Detectors with Different Backbones

Tab. 11 shows the performance of baseline detectors with different backbone networks. Similar to the results on SODA-D, we can see that ResNet-101 only brings slight performance improvement even decline. However, when Swin-T backbone was employed to extract the features, two fundamentally distinct phenomena occur simultaneously. For RPN-based detectors, Swin-T can yield varying levels of performance gain (from 0.1 points to 1.2 points), but for RPN-free detectors, Swin-T causes substantial performance decline (-3.8 points for Rotated RetinaNet and -2.5 points



Fig. 12. Qualitative results of Oriented RCNN [159] on SODA-A test-set. Columns 1 and 3 represent the ground-truth annotations and columns 2 and 4 denote the predictions. Best viewed in color. Only predictions with confidence scores larger than 0.3 are demonstrated.

for S²A-Net), which is completely different from the results on SODA-D. We conjecture this disparity lies in the limited ability of Swin-T to cope with dense distribution when the detector suffers from misalignment issue, particularly for those objects with extremely close proximity.

5.4.4 Number of Proposals

As we alluded to before, the objects in our SODA-A may distribute in a very dense fashion, which actually requires deliberate settings about proposal parameters. Intuitively, we have to strike a balance between proposal numbers and detection accuracy, in other words, computational consumption and accuracy. Excessive proposals could ensure the recall rate, though, it involves massive computation concurrently. While inadequate proposals hinder the overall performance. To determine the optimal choice about patch-level proposal numbers for best performance on SODA-A, we train Oriented RCNN (with a ResNet-50 as backbone network) with train-set and test on the test-set. Tab. 12 reports the results with different proposal number settings. We can see that the AP and AP_T performance vary slightly when the proposal numbers change from 2000 to 8000, whereas the detection speed decreases dramatically. Hence we set the proposal number to 2000 for optimal performance, both accuracy and speed, in our experiments.

5.4.5 Qualitative Results

We visualize the detection results of Oriented RCNN on SODA-D test-set in Fig. 12. The first pair shows the results of tiny instances and only very few of them were detected, demonstrating that the detection of tiny objects is a massive challenge for current detectors, even with top performance. The second pair exhibits the detections of low contrast, of which *airplane* instances possess similar visual feature with background and the model confuses them with *helicopter*. Moreover, because the detailed information which is conducive for identification and localization is hardly retained, the model is likely to utilize visual appearance for recognition instead, which unavoidably results in false positives and incorrect predictions (see the *container* predictions).

6 CONCLUSION AND OUTLOOK

We presented a systematic study on small object detection. Concretely, we exhaustively reviewed hundreds of literature for SOD from the perspective of algorithms and datasets.

Moreover, to catalyze the progress of SOD, we constructed two large-scale benchmarks under driving scenario and aerial scene, dubbed SODA-D and SODA-A. SODA-D comprises 277596 instances annotated with horizontal boxes, while SODA-A includes 800203 objects with oriented boxes. The well-annotated datasets, to the best of our knowledge, are the first attempt to large-scale benchmarks tailored for small object detection, and could serve as an impartial platform for benchmarking various SOD methods. On top of SODA, we performed a thorough evaluation and comparison of several representative algorithms. Based on the results, we discuss several potential solutions and directions for future development of SOD task.

Effective backbone. As alluded to in the results, deeper backbone networks might not be conducive to extract high-quality feature representations for small objects. Designing an effective backbone, which enjoys powerful feature extraction capability while avoiding high computational cost and information loss, is of paramount importance.

Efficient hierarchical feature representation. FPN is an indispensable part in small object detection. Nevertheless, current feature pyramid architecture is suboptimal for SOD, where top layers are redundant and unused owing to the heuristic pyramid level assign strategy. Moreover, detecting on low-level feature maps brings heavy computational burden. Thus, an efficient hierarchical feature architecture tailored for SOD task is in high demand.

Powerful single-shot detector for SOD. There exists a remarkable performance gap between two-stage detectors and one-stage ones, while the latter is of significance in real-world scenarios owing to their high computational efficiency. Also the common imbalance and misalignment issues suffered in one-stage methods are magnified when it comes to the small object detection. Therefore, a powerful single-shot SOD paradigm is crucial for both research and application.

ACKNOWLEDGMENTS

We thank Peter Kuntschieder for the constructive discussions and feedback, as well as their high-quality Mapillary Vistas Dataset.

REFERENCES

- [1] S. Ren, K. He, R. Girshick, and J. Sun, “Faster r-cnn: Towards real-time object detection with region proposal networks,” *TPAMI*, vol. 39, no. 6, pp. 1137–1149, 2017.

[2] T. Lin, P. Dollár, R. Girshick, K. He, B. Hariharan, and S. Belongie, "Feature pyramid networks for object detection," in *CVPR*, 2017, pp. 2117–2125.

[3] T. Lin, P. Goyal, R. Girshick, K. He, and P. Dollár, "Focal loss for dense object detection," *TPAMI*, vol. 42, no. 2, pp. 318–327, 2020.

[4] Z. Tian, C. Shen, H. Chen, and T. He, "Fcos: A simple and strong anchor-free object detector," *TPAMI*, vol. 44, no. 4, pp. 1922–1933, 2022.

[5] N. Carion, F. Massa, G. Synnaeve, N. Usunier, A. Kirillov, and S. Zagoruyko, "End-to-end object detection with transformers," in *ECCV*, 2020, pp. 213–229.

[6] T. Lin, M. Maire, S. Belongie, J. Hays, P. Perona, D. Ramanan, P. Dollár, and C. L. Zitnick, "Microsoft coco: Common objects in context," in *ECCV*, 2014, pp. 740–755.

[7] X. Yu, Y. Gong, N. Jiang, Q. Ye, and Z. Han, "Scale match for tiny person detection," in *WACV*, 2020, pp. 1257–1265.

[8] S. Yang, P. Luo, C. C. Loy, and X. Tang, "Wider face: A face detection benchmark," in *CVPR*, 2016, pp. 5525–5533.

[9] X. Dai, Y. Chen, B. Xiao, D. Chen, M. Liu, L. Yuan, and L. Zhang, "Dynamic head: Unifying object detection heads with attentions," in *CVPR*, 2021, pp. 7373–7382.

[10] K. He, X. Zhang, S. Ren, and J. Sun, "Deep residual learning for image recognition," in *CVPR*, 2016, pp. 770–778.

[11] S. Xie, R. Girshick, P. Dollár, Z. Tu, and K. He, "Aggregated residual transformations for deep neural networks," in *CVPR*, 2017, pp. 1492–1500.

[12] S.-H. Gao, M.-M. Cheng, K. Zhao, X.-Y. Zhang, M.-H. Yang, and P. Torr, "Res2net: A new multi-scale backbone architecture," *TPAMI*, vol. 43, no. 2, pp. 652–662, 2021.

[13] L. Liu, W. Ouyang, X. Wang, P. Fieguth, J. Chen, X. Liu, and M. Pietikäinen, "Deep learning for generic object detection: A survey," *IJCV*, vol. 128, no. 2, pp. 261–318, 2020.

[14] Z.-Q. Zhao, P. Zheng, S.-t. Xu, and X. Wu, "Object detection with deep learning: A review," *TNNLS*, vol. 30, no. 11, pp. 3212–3232, 2019.

[15] D. Geronimo, A. M. Lopez, A. D. Sappa, and T. Graf, "Survey of pedestrian detection for advanced driver assistance systems," *TPAMI*, vol. 32, no. 7, pp. 1239–1258, 2009.

[16] P. Dollar, C. Wojek, B. Schiele, and P. Perona, "Pedestrian detection: An evaluation of the state of the art," *TPAMI*, vol. 34, no. 4, pp. 743–761, 2011.

[17] J. Cao, Y. Pang, J. Xie, F. S. Khan, and L. Shao, "From handcrafted to deep features for pedestrian detection: A survey," *TPAMI*, pp. 1–1, 2021.

[18] Q. Ye and D. Doermann, "Text detection and recognition in imagery: A survey," *TPAMI*, vol. 37, no. 7, pp. 1480–1500, 2014.

[19] G. Cheng and J. Han, "A survey on object detection in optical remote sensing images," *ISPRS J. Photogramm. Remote Sens.*, vol. 117, pp. 11–28, 2016.

[20] K. Li, G. Wan, G. Cheng, L. Meng, and J. Han, "Object detection in optical remote sensing images: A survey and a new benchmark," *ISPRS J. Photogramm. Remote Sens.*, vol. 159, pp. 296–307, 2020.

[21] M. B. Jensen, M. P. Philipsen, A. Møgelmose, T. B. Moeslund, and M. M. Trivedi, "Vision for looking at traffic lights: Issues, survey, and perspectives," *IEEE Trans. Intell. Transp. Syst.*, vol. 17, no. 7, pp. 1800–1815, 2016.

[22] A. Boukerche and Z. Hou, "Object detection using deep learning methods in traffic scenarios," *ACM Comput Surv.*, vol. 54, no. 2, pp. 1–35, 2021.

[23] K. Oksuz, B. C. Cam, S. Kalkan, and E. Akbas, "Imbalance problems in object detection: A review," *TPAMI*, vol. 43, no. 10, pp. 3388–3415, 2020.

[24] D. Zhang, J. Han, G. Cheng, and M.-H. Yang, "Weakly supervised object localization and detection: A survey," *TPAMI*, pp. 1–1, 2021.

[25] K. Tong, Y. Wu, and F. Zhou, "Recent advances in small object detection based on deep learning: A review," *Image Vis Comput.*, vol. 97, p. 103910, 2020.

[26] Y. Liu, P. Sun, N. Wergeles, and Y. Shang, "A survey and performance evaluation of deep learning methods for small object detection," *Expert Syst. Appl.*, vol. 172, p. 114602, 2021.

[27] G. Chen, H. Wang, K. Chen, Z. Li, Z. Song, Y. Liu, W. Chen, and A. Knoll, "A survey of the four pillars for small object detection: Multiscale representation, contextual information, super-resolution, and region proposal," *IEEE Trans. Syst., Man, Cybern. Syst.*, vol. 52, no. 2, pp. 936–953, 2022.

[28] C. Chen, M.-Y. Liu, O. Tuzel, and J. Xiao, "R-cnn for small object detection," in *ACCV*, 2016, pp. 214–230.

[29] X. Yu, P. Chen, D. Wu, N. Hassan, G. Li, J. Yan, H. Shi, Q. Ye, and Z. Han, "Object localization under single coarse point supervision," in *CVPR*, 2022, pp. 4868–4877.

[30] J. Ding, N. Xue, G.-S. Xia, X. Bai, W. Yang, M. Yang, S. Belongie, J. Luo, M. Datcu, M. Pelillo, and L. Zhang, "Object detection in aerial images: A large-scale benchmark and challenges," *TPAMI*, pp. 1–1, 2021.

[31] M. Everingham, L. Van Gool, C. K. Williams, J. Winn, and A. Zisserman, "The pascal visual object classes (voc) challenge," *IJCV*, vol. 88, no. 2, pp. 303–338, 2010.

[32] J. Deng, W. Dong, R. Socher, L.-J. Li, K. Li, and L. Fei-Fei, "Imagenet: A large-scale hierarchical image database," in *CVPR*, 2009, pp. 248–255.

[33] G. Neuhold, T. Ollmann, S. R. Bulò, and P. Kortscheder, "The mapillary vistas dataset for semantic understanding of street scenes," in *ICCV*, 2017, pp. 5000–5009.

[34] D. G. Lowe, "Distinctive image features from scale-invariant keypoints," *IJCV*, vol. 60, no. 2, pp. 91–110, 2004.

[35] N. Dalal and B. Triggs, "Histograms of oriented gradients for human detection," in *CVPR*, 2005, pp. 886–893.

[36] H. Bay, A. Ess, T. Tuytelaars, and L. Van Gool, "Speeded-up robust features (surf)," *Comput Vis Image Underst.*, vol. 110, no. 3, pp. 346–359, 2008.

[37] C. Cortes and V. Vapnik, "Support-vector networks," *Mach Learn.*, vol. 20, no. 3, pp. 273–297, 1995.

[38] T. K. Ho, "Random decision forests," in *ICDAR*, 1995, pp. 278–282.

[39] A. Krizhevsky, I. Sutskever, and G. E. Hinton, "Imagenet classification with deep convolutional neural networks," in *NeurIPS*, 2012, pp. 1097–1105.

[40] R. Girshick, J. Donahue, T. Darrell, and J. Malik, "Region-based convolutional networks for accurate object detection and segmentation," *TPAMI*, vol. 38, no. 1, pp. 142–158, 2015.

[41] H. Noh, S. Hong, and B. Han, "Learning deconvolution network for semantic segmentation," in *ICCV*, 2015, pp. 1520–1528.

[42] L. Chen, H. Zheng, Z. Yan, and Y. Li, "Discriminative region mining for object detection," *TMM*, vol. 23, pp. 4297–4310, 2021.

[43] Z. Qin, Z. Li, Z. Zhang, Y. Bao, G. Yu, Y. Peng, and J. Sun, "Thundernet: Towards real-time generic object detection on mobile devices," in *ICCV*, 2019, pp. 6717–6726.

[44] J. Redmon, S. Divvala, R. Girshick, and A. Farhadi, "You only look once: Unified, real-time object detection," in *CVPR*, 2016, pp. 779–788.

[45] J. Redmon and A. Farhadi, "Yolov3: An incremental improvement," *arXiv preprint arXiv:1804.02767*, 2018.

[46] R. Girshick, "Fast r-cnn," in *ICCV*, 2015, pp. 1440–1448.

[47] X. Zhou, D. Wang, and P. Krähenbühl, "Objects as points," *arXiv preprint arXiv:1904.07850*, 2019.

[48] K. He, X. Zhang, S. Ren, and J. Sun, "Spatial pyramid pooling in deep convolutional networks for visual recognition," *TPAMI*, vol. 37, no. 9, pp. 1904–1916, 2015.

[49] W. Liu, D. Anguelov, D. Erhan, C. Szegedy, S. Reed, C.-Y. Fu, and A. C. Berg, "Ssd: Single shot multibox detector," in *ECCV*, 2016, pp. 21–37.

[50] K. Duan, S. Bai, L. Xie, H. Qi, Q. Huang, and Q. Tian, "Centernet: Keypoint triplets for object detection," in *ICCV*, 2019, pp. 6569–6578.

[51] H. Law and J. Deng, "Cornernet: Detecting objects as paired keypoints," in *ECCV*, 2018, pp. 734–750.

[52] X. Zhu, W. Su, L. Lu, B. Li, X. Wang, and J. Dai, "Deformable detr: Deformable transformers for end-to-end object detection," in *ICLR*, 2020.

[53] M. Kisantal, Z. Wojna, J. Murawski, J. Naruniec, and K. Cho, "Augmentation for small object detection," *arXiv preprint arXiv:1902.07296*, 2019.

[54] C. Chen, Y. Zhang, Q. Lv, S. Wei, X. Wang, X. Sun, and J. Dong, "Rrnet: A hybrid detector for object detection in drone-captured images," in *ICCVW*, 2019, pp. 100–108.

[55] A. Bochkovskiy, C.-Y. Wang, and H.-Y. M. Liao, "Yolov4: Optimal speed and accuracy of object detection," *arXiv preprint arXiv:2004.10934*, 2020.

[56] Z. Wei, C. Duan, X. Song, Y. Tian, and H. Wang, "Amrnet: Chips augmentation in aerial images object detection," *arXiv preprint arXiv:2009.07168*, 2020.

[57] C. Duan, Z. Wei, C. Zhang, S. Qu, and H. Wang, "Coarse-grained density map guided object detection in aerial images," in *ICCVW*, 2021, pp. 2789–2798.

[58] B. Zoph, E. D. Cubuk, G. Ghiasi, T.-Y. Lin, J. Shlens, and Q. V. Le, "Learning data augmentation strategies for object detection," in *ECCV*, 2020, pp. 566–583.

[59] B. Zoph and Q. V. Le, "Neural architecture search with reinforcement learning," *arXiv preprint arXiv:1611.01578*, 2016.

[60] E. D. Cubuk, B. Zoph, J. Shlens, and Q. V. Le, "RandAugment: Practical automated data augmentation with a reduced search space," in *CVPRW*, 2020, pp. 3008–3017.

[61] P. Dollár, R. Appel, S. Belongie, and P. Perona, "Fast feature pyramids for object detection," *TPAMI*, vol. 36, no. 8, pp. 1532–1545, 2014.

[62] P. F. Felzenszwalb, R. B. Girshick, D. McAllester, and D. Ramanan, "Object detection with discriminatively trained part-based models," *TPAMI*, vol. 32, no. 9, pp. 1627–1645, 2010.

[63] E. H. Adelson, C. H. Anderson, J. R. Bergen, P. J. Burt, and J. M. Ogden, "Pyramid methods in image processing," *RCA engineer*, vol. 29, no. 6, pp. 33–41, 1984.

[64] B. Hariharan, P. Arbelaez, R. Girshick, and J. Malik, "Object instance segmentation and fine-grained localization using hypercolumns," *TPAMI*, vol. 39, no. 4, pp. 627–639, 2016.

[65] H. Zhao, J. Shi, X. Qi, X. Wang, and J. Jia, "Pyramid scene parsing network," in *CVPR*, 2017, pp. 6230–6239.

[66] T. Kong, A. Yao, Y. Chen, and F. Sun, "Hypernet: Towards accurate region proposal generation and joint object detection," in *CVPR*, 2016, pp. 845–853.

[67] F. Yang, W. Choi, and Y. Lin, "Exploit all the layers: Fast and accurate cnn object detector with scale dependent pooling and cascaded rejection classifiers," in *CVPR*, 2016, pp. 2129–2137.

[68] Z. Cai, Q. Fan, R. S. Feris, and N. Vasconcelos, "A unified multi-scale deep convolutional neural network for fast object detection," in *ECCV*, 2016, pp. 354–370.

[69] J. Li, Y. Wang, C. Wang, Y. Tai, J. Qian, J. Yang, C. Wang, J. Li, and F. Huang, "Dsfd: Dual shot face detector," in *CVPR*, 2019, pp. 5055–5064.

[70] Q. Zhao, T. Sheng, Y. Wang, Z. Tang, Y. Chen, L. Cai, and H. Ling, "M2det: A single-shot object detector based on multi-level feature pyramid network," in *AAAI*, 2019, pp. 9259–9266.

[71] J. Li, X. Liang, S. Shen, T. Xu, J. Feng, and S. Yan, "Scale-aware fast r-cnn for pedestrian detection," *TMM*, vol. 20, no. 4, pp. 985–996, 2017.

[72] M. Najibi, P. Samangouei, R. Chellappa, and L. S. Davis, "Ssh: Single stage headless face detector," in *ICCV*, 2017, pp. 4885–4894.

[73] Y. Li, Y. Chen, N. Wang, and Z.-X. Zhang, "Scale-aware trident networks for object detection," in *ICCV*, 2019, pp. 6053–6062.

[74] S. Liu, L. Qi, H. Qin, J. Shi, and J. Jia, "Path aggregation network for instance segmentation," in *CVPR*, 2018, pp. 8759–8768.

[75] H. Zhang, K. Wang, Y. Tian, C. Gou, and F.-Y. Wang, "Mfr-cnn: Incorporating multi-scale features and global information for traffic object detection," *IEEE Trans. Veh. Technol.*, vol. 67, no. 9, pp. 8019–8030, 2018.

[76] C. Yang, Z. Huang, and N. Wang, "Querydet: Cascaded sparse query for accelerating high-resolution small object detection," in *CVPR*, 2022, pp. 13 668–13 677.

[77] J. Huang *et al.*, "Speed/accuracy trade-offs for modern convolutional object detectors," in *CVPR*, 2017, pp. 3296–3297.

[78] B. Singh and L. S. Davis, "An analysis of scale invariance in object detection-snip," in *CVPR*, 2018, pp. 3578–3587.

[79] B. Singh, M. Najibi, and L. S. Davis, "Sniper: Efficient multi-scale training," in *NeurIPS*, vol. 31, 2018.

[80] M. Najibi, B. Singh, and L. Davis, "Autofocus: Efficient multi-scale inference," in *ICCV*, 2019, pp. 9745–9755.

[81] Y. Chen, P. Zhang, Z. Li, Y. Li, X. Zhang, L. Qi, J. Sun, and J. Jia, "Dynamic scale training for object detection," *arXiv preprint arXiv:2004.12432*, 2020.

[82] P. Zhou, B. Ni, C. Geng, J. Hu, and Y. Xu, "Scale-transferrable object detection," in *CVPR*, 2018, pp. 528–537.

[83] J. Wang, Y. Yuan, and G. Yu, "Face attention network: An effective face detector for the occluded faces," *arXiv preprint arXiv:1711.07246*, 2017.

[84] A. Shrivastava, R. Sukthankar, J. Malik, and A. Gupta, "Beyond skip connections: Top-down modulation for object detection," *arXiv preprint arXiv:1612.06851*, 2016.

[85] M. Zand, A. Etemad, and M. Greenspan, "Oriented bounding boxes for small and freely rotated objects," *IEEE Trans. Geosci. Remote Sens.*, vol. 60, pp. 1–15, 2021.

[86] S. Woo, S. Hwang, and I. S. Kweon, "Stairnet: Top-down semantic aggregation for accurate one shot detection," in *WACV*, 2018, pp. 1093–1102.

[87] Y. Gong, X. Yu, Y. Ding, X. Peng, J. Zhao, and Z. Han, "Effective fusion factor in fpn for tiny object detection," in *WACV*, 2021, pp. 1159–1167.

[88] M. Hong, S. Li, Y. Yang, F. Zhu, Q. Zhao, and L. Lu, "Sspnet: Scale selection pyramid network for tiny person detection from uav images," *IEEE Geosci. Remote. Sens. Lett.*, vol. 19, pp. 1–5, 2021.

[89] C.-Y. Fu, W. Liu, A. Ranga, A. Tyagi, and A. C. Berg, "Dssd: Deconvolutional single shot detector," *arXiv preprint arXiv:1701.06659*, 2017.

[90] Z. Liu, G. Gao, L. Sun, and L. Fang, "Ipg-net: Image pyramid guidance network for small object detection," in *CVPRW*, 2020, pp. 4422–4430.

[91] S. Liu, D. Huang, and Y. Wang, "Learning spatial fusion for single-shot object detection," *arXiv preprint arXiv:1911.09516*, 2019.

[92] P. Hu and D. Ramanan, "Finding tiny faces," in *CVPR*, 2017, pp. 1522–1530.

[93] M. Haris, G. Shakhnarovich, and N. Ukita, "Task-driven super resolution: Object detection in low-resolution images," in *NeurIPS*, 2021, pp. 387–395.

[94] J. Wang, K. Chen, R. Xu, Z. Liu, C. C. Loy, and D. Lin, "Carafe: Content-aware reassembly of features," in *ICCV*, 2019, pp. 3007–3016.

[95] I. J. Goodfellow, J. Pouget-Abadie, M. Mirza, B. Xu, D. Warde-Farley, S. Ozair, A. C. Courville, and Y. Bengio, "Generative adversarial nets," in *NeurIPS*, 2014, pp. 2672–2680.

[96] C. Deng, M. Wang, L. Liu, Y. Liu, and Y. Jiang, "Extended feature pyramid network for small object detection," *TMM*, vol. 24, pp. 1968–1979, 2021.

[97] W. Shi, J. Caballero, F. Huszár, J. Totz, A. P. Aitken, R. Bishop, D. Rueckert, and Z. Wang, "Real-time single image and video super-resolution using an efficient sub-pixel convolutional neural network," in *CVPR*, 2016, pp. 1874–1883.

[98] Y. Bai, Y. Zhang, M. Ding, and B. Ghanem, "Sod-mtgan: Small object detection via multi-task generative adversarial network," in *ECCV*, 2018, pp. 210–226.

[99] —, "Finding tiny faces in the wild with generative adversarial network," in *CVPR*, 2018, pp. 21–30.

[100] B. Na and G. C. Fox, "Object detection by a super-resolution method and a convolutional neural networks," in *BigData*, 2018, pp. 2263–2269.

[101] J. Noh, W. Bae, W. Lee, J. Seo, and G. Kim, "Better to follow, follow to be better: Towards precise supervision of feature super-resolution for small object detection," in *ICCV*, 2019, pp. 9724–9733.

[102] S. K. Divvala, D. Hoiem, J. H. Hays, A. A. Efros, and M. Hebert, "An empirical study of context in object detection," in *CVPR*, 2009, pp. 1271–1278.

[103] J. Li, X. Liang, Y. Wei, T. Xu, J. Feng, and S. Yan, "Perceptual generative adversarial networks for small object detection," in *CVPR*, 2017, pp. 1951–1959.

[104] A. Torralba, "Contextual priming for object detection," *IJCV*, vol. 53, no. 2, pp. 169–191, 2003.

[105] X. Tang, D. K. Du, Z. He, and J. Liu, "Pyramidbox: A context-assisted single shot face detector," in *ECCV*, 2018, pp. 812–828.

[106] D. Parikh, C. L. Zitnick, and T. Chen, "Exploring tiny images: The roles of appearance and contextual information for machine and human object recognition," *TPAMI*, vol. 34, no. 10, pp. 1978–1991, 2011.

[107] H. Zhang, K. Dana, J. Shi, Z. Zhang, X. Wang, A. Tyagi, and A. Agrawal, "Context encoding for semantic segmentation," in *CVPR*, 2018, pp. 7151–7160.

[108] K. Chen, J. Pang, J. Wang, Y. Xiong, X. Li, S. Sun, W. Feng, Z. Liu, J. Shi, W. Ouyang *et al.*, "Hybrid task cascade for instance segmentation," in *CVPR*, 2019, pp. 4969–4978.

[109] X. Liang, J. Zhang, L. Zhuo, Y. Li, and Q. Tian, "Small object detection in unmanned aerial vehicle images using feature fusion and scaling-based single shot detector with spatial context analysis," *TCSVT*, vol. 30, no. 6, pp. 1758–1770, 2020.

[110] X. Hu, X. Xu, Y. Xiao, H. Chen, S. He, J. Qin, and P.-A. Heng, "Sinet: A scale-insensitive convolutional neural network for fast vehicle detection," *IEEE Trans. Intell. Transp. Syst.*, vol. 20, no. 3, pp. 1010–1019, 2019.

[111] S. Bell, C. L. Zitnick, K. Bala, and R. Girshick, "Inside-outside net: Detecting objects in context with skip pooling and recurrent neural networks," in *CVPR*, 2016, pp. 2874–2883.

[112] Q. V. Le, N. Jaitly, and G. E. Hinton, "A simple way to initialize recurrent networks of rectified linear units," *arXiv preprint arXiv:1504.00941*, 2015.

[113] M. Braun, S. Krebs, F. Flohr, and D. M. Gavrila, "Eurocity persons: A novel benchmark for person detection in traffic scenes," *TPAMI*, vol. 41, no. 8, pp. 1844–1861, 2019.

[114] S. Zhang, Y. Xie, J. Wan, H. Xia, S. Z. Li, and G. Guo, "Wider-person: A diverse dataset for dense pedestrian detection in the wild," *TMM*, vol. 22, no. 2, pp. 380–393, 2020.

[115] Z. Zhu, D. Liang, S. Zhang, X. Huang, B. Li, and S. Hu, "Traffic-sign detection and classification in the wild," in *CVPR*, 2016, pp. 2110–2118.

[116] J. Wang, W. Yang, H. Guo, R. Zhang, and G.-S. Xia, "Tiny object detection in aerial images," in *ICPR*, 2021, pp. 3791–3798.

[117] Q. Wang, J. Gao, W. Lin, and X. Li, "Nwpu-crowd: A large-scale benchmark for crowd counting and localization," *TPAMI*, vol. 43, no. 6, pp. 2141–2149, 2021.

[118] A. Borji and L. Itti, "State-of-the-art in visual attention modeling," *TPAMI*, vol. 35, no. 1, pp. 185–207, 2012.

[119] W. Wang, J. Shen, X. Lu, S. C. H. Hoi, and H. Ling, "Paying attention to video object pattern understanding," *TPAMI*, vol. 43, no. 7, pp. 2413–2428, 2021.

[120] L. Itti, C. Koch, and E. Niebur, "A model of saliency-based visual attention for rapid scene analysis," *TPAMI*, vol. 20, no. 11, pp. 1254–1259, 1998.

[121] M. Corbetta and G. L. Shulman, "Control of goal-directed and stimulus-driven attention in the brain," *Nat. Rev. Neurosci*, vol. 3, no. 3, pp. 201–215, 2002.

[122] X. Wang, R. Girshick, A. Gupta, and K. He, "Non-local neural networks," in *CVPR*, 2018, pp. 7794–7803.

[123] S. Woo, J. Park, J.-Y. Lee, and I. S. Kweon, "Cbam: Convolutional block attention module," in *ECCV*, 2018, pp. 3–19.

[124] J. Hu, L. Shen, and G. Sun, "Squeeze-and-excitation networks," in *CVPR*, 2018, pp. 7132–7141.

[125] M. Jaderberg, K. Simonyan, A. Zisserman *et al.*, "Spatial transformer networks," in *NeurIPS*, 2015, pp. 2017–2025.

[126] A. Vaswani, N. Shazeer, N. Parmar, J. Uszkoreit, L. Jones, A. N. Gomez, L. Kaiser, and I. Polosukhin, "Attention is all you need," in *NeurIPS*, 2017, pp. 6000–6010.

[127] C. Feng, Y. Zhong, Y. Gao, M. R. Scott, and W. Huang, "Tood: Task-aligned one-stage object detection," in *ICCV*, 2021, pp. 3490–3499.

[128] Z. Huang, X. Wang, L. Huang, C. Huang, Y. Wei, and W. Liu, "Ccnet: Criss-cross attention for semantic segmentation," in *ICCV*, 2019, pp. 603–612.

[129] J. Pang, C. Li, J. Shi, Z. Xu, and H. Feng, " \mathcal{R}^2 -cnn: Fast tiny object detection in large-scale remote sensing images," *IEEE Trans. Geosci. Remote Sens.*, vol. 57, no. 8, pp. 5512–5524, 2019.

[130] X. Yang, J. Yang, J. Yan, Y. Zhang, T. Zhang, Z. Guo, X. Sun, and K. Fu, "Scrdet: Towards more robust detection for small, cluttered and rotated objects," in *ICCV*, 2019, pp. 8231–8240.

[131] J. Fu, X. Sun, Z. Wang, and K. Fu, "An anchor-free method based on feature balancing and refinement network for multiscale ship detection in sar images," *IEEE Trans. Geosci. Remote Sens.*, vol. 59, no. 2, pp. 1331–1344, 2021.

[132] Y. Zhu, H. Cai, S. Zhang, C. Wang, and Y. Xiong, "Tinaface: Strong but simple baseline for face detection," *arXiv preprint arXiv:2011.13183*, 2020.

[133] Z. Zheng, P. Wang, W. Liu, J. Li, R. Ye, and D. Ren, "Distance-iou loss: Faster and better learning for bounding box regression," in *AAAI*, 2020, pp. 12 993–13 000.

[134] C. Xu, J. Wang, W. Yang, and L. Yu, "Dot distance for tiny object detection in aerial images," in *CVPRW*, 2021, pp. 1192–1201.

[135] J. Wang, C. Xu, W. Yang, and L. Yu, "A normalized gaussian wasserstein distance for tiny object detection," *arXiv preprint arXiv:2110.13389*, 2021.

[136] F. Yang, H. Fan, P. Chu, E. Blasch, and H. Ling, "Clustered object detection in aerial images," in *ICCV*, 2019, pp. 8311–8320.

[137] C. Li, T. Yang, S. Zhu, C. Chen, and S. Guan, "Density map guided object detection in aerial images," in *CVPRW*, 2020, pp. 737–746.

[138] T. Song, L. Sun, D. Xie, H. Sun, and S. Pu, "Small-scale pedestrian detection based on topological line localization and temporal feature aggregation," in *ECCV*, 2018, pp. 536–551.

[139] J. Wu, C. Zhou, Q. Zhang, M. Yang, and J. Yuan, "Self-mimic learning for small-scale pedestrian detection," in *ACM MM*, 2020, pp. 2012–2020.

[140] J. U. Kim, S. Park, and Y. M. Ro, "Robust small-scale pedestrian detection with cued recall via memory learning," in *ICCV*, 2021, pp. 3030–3039.

[141] G. Cheng, J. Wang, K. Li, X. Xie, C. Lang, Y. Yao, and J. Han, "Anchor-free oriented proposal generator for object detection," *IEEE Trans. Geosci. Remote Sens.*, vol. 60, pp. 1–11, 2022.

[142] Y. Pang, J. Cao, Y. Li, J. Xie, H. Sun, and J. Gong, "Tju-dhd: A diverse high-resolution dataset for object detection," *TIP*, vol. 30, pp. 207–219, 2021.

[143] J. Han, X. Liang, H. Xu, K. Chen, L. Hong, J. Mao, C. Ye, W. Zhang, Z. Li, X. Liang *et al.*, "Soda10m: A large-scale 2d self/semi-supervised object detection dataset for autonomous driving," *arXiv preprint arXiv:2106.11118*, 2021.

[144] M.-R. Hsieh, Y.-L. Lin, and W. H. Hsu, "Drone-based object counting by spatially regularized regional proposal network," in *ICCV*, 2017, pp. 4165–4173.

[145] P. Zhu, L. Wen, D. Du, X. Bian, H. Fan, Q. Hu, and H. Ling, "Detection and tracking meet drones challenge," *TPAMI*, pp. 1–1, 2021.

[146] D.-P. Fan, G.-P. Ji, M.-M. Cheng, and L. Shao, "Concealed object detection," *TPAMI*, pp. 1–1, 2021.

[147] W. Wang, J. Shen, F. Guo, M.-M. Cheng, and A. Borji, "Revisiting video saliency: A large-scale benchmark and a new model," in *CVPR*, 2018, pp. 4894–4903.

[148] H. Yu, G. Li, W. Zhang, Q. Huang, D. Du, Q. Tian, and N. Sebe, "The unmanned aerial vehicle benchmark: Object detection, tracking and baseline," *IJCV*, vol. 128, no. 5, pp. 1141–1159, 2020.

[149] Z. Cai and N. Vasconcelos, "Cascade r-cnn: High quality object detection and instance segmentation," *TPAMI*, vol. 43, no. 5, pp. 1483–1498, 2021.

[150] D. Lam, R. Kuzma, K. McGee, S. Dooley, M. Laielli, M. Klaric, Y. Bulatov, and B. McCord, "xview: Objects in context in overhead imagery," *arXiv preprint arXiv:1802.07856*, 2018.

[151] Z. Yang, S. Liu, H. Hu, L. Wang, and S. Lin, "Reppoints: Point set representation for object detection," in *ICCV*, 2019, pp. 9656–9665.

[152] S. Zhang, C. Chi, Y. Yao, Z. Lei, and S. Z. Li, "Bridging the gap between anchor-based and anchor-free detection via adaptive training sample selection," in *CVPR*, 2020, pp. 9759–9768.

[153] P. Sun, R. Zhang, Y. Jiang, T. Kong, C. Xu, W. Zhan, M. Tomizuka, L. Li, Z. Yuan, C. Wang, and P. Luo, "Sparse r-cnn: End-to-end object detection with learnable proposals," in *CVPR*, 2021, pp. 14 449–14 458.

[154] K. Chen *et al.*, "MMDetection: Open mmlab detection toolbox and benchmark," *arXiv preprint arXiv:1906.07155*, 2019.

[155] Y. Zhou *et al.*, "Mmrotate: A rotated object detection benchmark using pytorch," *arXiv preprint arXiv:2204.13317*, 2022.

[156] Z. Liu, Y. Lin, Y. Cao, H. Hu, Y. Wei, Z. Zhang, S. Lin, and B. Guo, "Swin transformer: Hierarchical vision transformer using shifted windows," in *ICCV*, 2021, pp. 9992–10 002.

[157] J. Ding, N. Xue, Y. Long, G.-S. Xia, and Q. Lu, "Learning roi transformer for oriented object detection in aerial images," in *CVPR*, 2019, pp. 2844–2853.

[158] Y. Xu, M. Fu, Q. Wang, Y. Wang, K. Chen, G.-S. Xia, and X. Bai, "Gliding vertex on the horizontal bounding box for multi-oriented object detection," *TPAMI*, vol. 43, no. 4, pp. 1452–1459, 2021.

[159] X. Xie, G. Cheng, J. Wang, X. Yao, and J. Han, "Oriented r-cnn for object detection," in *ICCV*, 2021, pp. 3520–3529.

[160] J. Han, J. Ding, J. Li, and G.-S. Xia, "Align deep features for oriented object detection," *IEEE Trans. Geosci. Remote Sens.*, vol. 60, pp. 1–11, 2022.

[161] G. Cheng, Y. Yao, S. Li, K. Li, X. Xie, J. Wang, X. Yao, and J. Han, "Dual-aligned oriented detector," *IEEE Trans. Geosci. Remote Sens.*, vol. 60, pp. 1–11, 2022.